NASA Technical Memorandum 84220

An Analysis of a Nonlinear Instability in the Implementation of a VTOL Control System During Hover

Jeanine M. Weber

March 1982

National Aeronautics and
Space Administration

NASA Technical Memorandum 84220

An Analysis of a Nonlinear Instability in the Implementation of a VTOL Control System During Hover

Jeanine M. Weber, Ames Research Center, Moffett Field, California

National Aeronautics and
Space Administration

Ames Research Center
Moffett Field, California 94035

TABLE OF CONTENTS

NOMENCLATURE

A	analytical limiter input (used in describing function analysis)
a	analytical limiter value (used in describing function analysis)
b_1/A	describing function gain
$DB_{\delta I\psi}$	deadband of rudder pedal deflection
$DB_{\psi H}$	deadband in rudder pedal integrator
FCN	rudder pedal to rudder gearing function and limiter
f_s	digital computer sampling frequency
G_Y	full authority series servo gain
GH(s)	open loop transfer function
I_z	moment of inertia about aircraft z-axis
K	root locus gain
K_B	control mode phase-out gain
Kr_ϕ	gain of roll attitude feedback into yaw controller
K_p	parallel/series servo mode combined analysis gain $= (K_{ps} \times K_{30} \times K_{YC} \times -1 \times FCN)$
K_{ps}	parallel servo gain
K_s	parallel/series servo mode combined analysis gain $= (K_{ss} \times K_{30})$
K_{ss}	series servo gain
K_{TORQUE}	actuation dynamics torque gain
K_{YC}	additional parallel servo gain
K_ψ	yaw attitude feedback gain
$K_{\dot\psi}$	yaw rate feedback gain
$K_{\psi H}$	pedal integrator gain

K_1	combined analysis gain = $(K_\psi \times K_{\psi_H})$
K_2	combined analysis gain = $(K_{10} + K_{20})$
K_3	full authority series servo mode combined analysis gain = $(K_{30} \times -1 \times G_Y \times FCN \times K_{TORQUE}/I_z)$
K_5	parallel/series servo mode combined analysis gain = (K_{TORQUE}/I_z)
K_{10}	yaw controller forward gain component
K_{20}	yaw controller forward gain component
K_{30}	yaw controller coupling gain
$LM_{\delta I_\psi}$	position limit of rudder pedals
LM_{ψ_c}	yaw controller coupling limit
SRFIMF	state-rate-feedback-implicit-model-following
T	digital computer sampling period
β	aircraft sideslip angle
$\dot{\beta}_I$	time derivative of inertial sideslip angle
δ_{I_ψ}	pilot control input to yaw controller (pedal input)
τ_2	actuation model time constant
τ_7	flight controller compensation time constant
ϕ	aircraft roll attitude
ψ	aircraft yaw attitude (heading)
$\dot{\psi}$	aircraft yaw rate
$\ddot{\psi}$	aircraft yaw acceleration
ψ_{AL}	experimental limiter output
ψ_{BL}	experimental limiter input

AN ANALYSIS OF A NONLINEAR INSTABILITY IN THE IMPLEMENTATION OF A VTOL CONTROL SYSTEM DURING HOVER

Jeanine M. Weber

NASA-Ames Research Center

SUMMARY

An analysis has been conducted to determine the contributions to nonlinear behavior and unstable response of the model following yaw control system of a VTOL aircraft during hover. The system was designed as a state rate feedback implicit model follower that provided yaw rate command/heading hold capability and used combined full authority parallel and limited authority series servo actuators to generate an input to the yaw reaction control system of the aircraft. Involved in the analysis were linear and nonlinear system models, and describing function linearization techniques to determine the influence of input magnitude and bandwidth, series servo authority and system bandwidth on the control system instability. Results of the analysis describe stability boundaries as a function of these system design characteristics.

INTRODUCTION

The use of advanced control systems that provide stabilization and command augmentation for attitude, translational velocity, and position control have been shown to reduce pilot workload for VTOL hover operations (references 1 and 2). One such example is the state-rate-feedback-implicit-model-following (SRFIMF) concept examined in reference 3, which achieves model-following fidelity through the feedback of acceleration, rate and attitude signals. In the ground simulation experiment of reference 3, this concept was shown to enhance the capability of the pilot-aircraft system to perform a demanding hover (and deceleration) task.

In-flight evaluation of several such control systems, including SRFIMF, with a VTOL research aircraft has been proposed. Toward that end, it is anticipated that the control system of an existing operational VTOL aircraft will be modified to permit incorporation of these concepts. In order to minimize the cost of implementation, a simplex electronic control system with manual override capability has been suggested. Safety considerations would be satisfied with a parallel/series servo arrangement of the actuators such that each servo is limited to contain a runaway failure. The parallel servo would be full authority and have a limited rate-of-actuation. The series servo would be position limited and capable of a high rate-of-actuation.

The reference 3 ground simulation assumed a full-authority fly-by-wire control system and did not address possible influences of the parallel/series servo mechanization on the SRFIMF control system. Hover simulation of the SRFIMF controller implemented in this manner during a control system failure study at Ames Research Center in August, 1979 (reference 4), revealed a nonlinear instability in the yaw axis. An electrical limiter in the control system, designed to limit the servo input upstream, saturated and cycled causing the divergent oscillation of the output signals. Although during the simulation, the instability was apparent only in the yaw axis, it is anticipated that there is a potential problem in any channel using the parallel/series mechanization.

The purpose of this study was to examine the causes and characteristics of this nonlinear instability. A describing function analysis technique (reference 5) was used in the study. Simplified linear and non-linear models of the controller, actuation and airframe dynamics were used to isolate and analyze the problem experimentally. The analysis encompassed only the wings-level hover flight condition.

This report presents the results of this analysis, including a description of the model with the appropriate simplifications, and analyses of the linear and nonlinear systems. The Nonlinear System Analysis portion involves a description of the system, theoretical and experimental approaches to understanding nominal system response, and experimentally establishing stability boundaries by varying system configuration.

MODEL DESCRIPTION

The SRFIMF yaw control system has been simplified for purposes of analysis. Included in the simplified model are the yaw flight controller, the option for selecting either parallel/series or full authority series servo implementation, actuation dynamics and yaw response of the aircraft which neglects aerodynamic effects.

Figure 1 shows the SRFIMF yaw control system as taken from figure 14 of reference 3. Shown in figure 2 is the yaw control system used in the analysis, which includes the following simplifications from the figure 1 model: deletion of the electrical deadbands on the pedal inputs to the system ($DB_{\delta I_\psi}$ and DB_{ψ_H}), deletion of the sideslip command mode (located downstream of the $\dot{\beta}_I$ and β inputs) which is active only for flight at or above 30 knots, and deletion of the tanϕ input path which is inapplicable to this wings-level analysis.

Figure 3 shows a block diagram of the simplified overall control system including servo implementation and actuation dynamics. The implementation flag selects either the parallel/series servo mode (1) or the full authority series servo mode (0). The limiter LM_{ψ_C} shown in figure 2 limits the servo input signal in the case of a runaway failure. A digital representation of the model shown in figures 2 and 3 was used in the analysis.

The problem has been analyzed in two parts: Initially the limiters were removed and the linear response was studied in each of the parallel/series and full authority series servo modes. The p ose of this was to understand the linear system response, and to verify the mplified Fortran model. The limiters were then introduced and the nonline response was analyzed theoretically with the describing function technique and experimentally using the time histories generated by the Fortran program.

LINEAR SYSTEM ANALYSIS

Linear System Classical Stability Analysis

This section describes the response characteristics of the linear system in terms of classical analysis techniques.

With further simplification, the block diagrams in figures 2 and 3 have been reduced to figures 4 and 5, representing the parallel/series and full authority series modes respectively.

Gain and signal equivalences between SRFIMF and the analysis, as well as the nominal gain values are given in the Appendix.

From figures 4 and 5 the open loop transfer functions of each mode can be written:

$$GH(s)\Big|_{\substack{\text{Parallel/Series}\\ \text{Servo Mode}\\ \text{(Linear System)}}} = \frac{K\left(\frac{K_s K_5}{\tau_2}\right)\left(s + \frac{1}{\tau_7}\right)\left(s + \frac{K_p}{K_s}\right)\left(s^2 + K_{\dot{\psi}} s + K_{\psi}\right)}{s^4\left(s + \frac{1}{\tau_2}\right)} \tag{1}$$

$$GH(s)\Big|_{\substack{\text{Series Servo}\\ \text{Mode}\\ \text{(Linear System)}}} = \frac{K\left(\frac{K_3}{\tau_2}\right)\left(s + \frac{1}{\tau_7}\right)\left(s^2 + K_{\dot{\psi}} s + K_{\psi}\right)}{s^3\left(s + \frac{1}{\tau_2}\right)} \tag{2}$$

where K is the open loop gain factor.

A root locus of the parallel/series mode is shown in figure 6 with partial root loci of each mode in figures 7 and 8 showing only the imaginary axis region. From figures 7 and 8 it is apparent that the system is conditionally stable in each mode, thus gain reduction is sufficient to destabilize the response. Note that in the parallel/series mode, the high frequency eigenvalues cross the imaginary axis at a higher gain value than in the series servo mode, thus the series servo mode remains stable at a lower effective

system gain. From equations (1) and (2) it can be seen that the series servo mode has three open loop integrators, whereas the parallel/series mode has four. In the nonlinear system, the extra integrator associated with the parallel/series servo implementation introduced a further destabilizing effect to the system.

Relative degrees of conditional stability between the modes are also illustrated using frequency response techniques. Figures 9 and 10 are Bode diagrams of the linear system. The higher gain and phase margin of the series servo mode indicate the increased resilience of that mode to system gain and phase angle reduction. From the figures it can be seen that the series servo mode becomes neutrally stable at the phase crossover frequency (2.2 rad/sec); above this frequency the system has a stable response. Due to the conditional stabiltiy of the system, if the Bode gain is reduced 21 db below the total loop gain of the design, the system becomes unstable. By contrast, the parallel/series servo mode has a phase crossover frequency of 4.5 rad/sec and the total loop gain can only be reduced by 11.6 db without destabilizing the system.

Computer Model Verification

The nominal sampling period, T, of the full Harrier simulation on the Xerox Sigma 9 computer is .05 sec, corresponding to a sampling frequency, fs, of 20 Hz. However, when the linearized model (limiters removed) is run at T = .05 sec, the characteristics of the time response are not equivalent to those predicted by the linear root locus analysis. When the sampling frequency is increased by a factor of ten (T = .005, f_s = 200 Hz), the time history characteristics compare well to those predicted by the linear analysis in the region of marginal to neutral stability. Figure 11 shows a comparison of the marginally stable mode characteristics as extracted from the time history responses run at T = .05, T = .005 and the linear analysis.

It is apparent from this comparison that the slower sampling frequency reduces the damping of this mode substantially and can lead to erroneous conclusions regarding system stability. Thus, for accuracy purposes, the analysis of this problem has been accomplished with a sampling period of T = .005 sec.

NONLINEAR SYSTEM ANALYSIS

Nonlinear Control System Elements

The non-linear control system includes limiters on series servo position and on the yaw reaction control.

The purpose of the first limiter is to arrest the series servo input to the yaw control actuator in the case of a series runaway failure. The limits are determined by the percentage of total control power that is acceptable to

be allotted to the series servo. The practical limits on series servo control power are a compromise between that required for effective control augmentation and that acceptable based on hard-over servo failure. With inputs of sufficient magnitudes and above specific frequencies the series servo was found to saturate and limit cycle, causing a divergent oscillation of the yaw response of the aircraft.

The yaw reaction control limit simply represents the total yawing moment control authority. This authority limit may be reached if the parallel actuator is driven to sufficiently large magnitudes by the pilot's control inputs or by unstable response in the yaw axis.

Describing Function Analysis

One tool for linearization and analysis of nonlinear control system elements is the describing function which is discussed in reference 5. The describing function of a simple limiter is:

$$\frac{b_1}{A} = \frac{2}{\pi}\left[\sin^{-1}\left(\frac{a}{A}\right) + \left(\frac{a}{A}\right)\sqrt{1 - \left(\frac{a}{A}\right)^2}\right] \tag{3}$$

where

$\frac{b_1}{A}$ = gain which replaces limiter in the linearization

$A = \psi_{BL}$ = magnitude of signal input to limiter

a = value to which output is limited

It can be seen from equation (3) that as the ratio of limiter size to signal magnitude, a/A, varies between 1 and 0, the describing function gain, b_1/A, varies between 1 and 0 also.

Shown in figure 12 is the parallel/series mode block diagram including the nonlinear element and, in equation (4), the open-loop transfer function with the equivalent linearized element. (A similar transfer function may be written for the series servo mode.)

$$GH(s)\Big|_{\substack{\text{Parallel/Series}\\ \text{Servo Mode}\\ \text{(Linearized}\\ \text{System)}}} = \frac{K\left(\frac{b_1}{A}\frac{K_s K_5}{\tau_2}\right)\left(s + \frac{1}{\tau_7}\right)\left(s + \frac{K_p}{K_s}\right)\left(s^2 + K_{\dot{\psi}}s + K_{\psi}\right)}{s^3\left(s + \frac{1 - \frac{b_1}{A}}{\tau_7}\right)\left(s + \frac{1}{\tau_2}\right)} \tag{4}$$

As the limit on servo command is reached and b_1/A decreases from the linear value of 1, the effects on the open loop transfer function are:

1. a reduction in system gain

2. movement of a pole from the origin along the negative real axis.

By solving the characteristic equation at discrete b_1/A values, the corresponding variation of the closed-loop roots of the system has been determined. Figures 13 and 14 show these root locations in each of the parallel/series and series servo modes respectively. In these figures, it may be seen that as b_1/A decreases from 1, a low frequency mode is introduced. The damping of this mode is reduced progressively as b_1/A approaches zero. In the parallel/series mode (figure 13), as b_1/A approaches zero, the closed-loop roots of the system approach those of the open-loop case that has three zeros at the origin. This leads to the low frequency eigenvalues being forced into the right half-plane. In figure 14, however, the closed-loop roots of the series system approach only two zeros at the origin as b_1/A approaches zero; thus, the root locus branches approach vertically and the eigenvalues always remain in the left half-plane.

It may be concluded that describing function gain value has a significant effect on system response and stability. Given system input, δ_{I_ψ}, the describing function gain value, b_1/A, may be found with the transfer function between system and limiter input, A/δ_{I_ψ}, given in equation (5).

$$\frac{\psi_{BL}}{\delta_{I_\psi}} = \frac{A}{\delta_{I_\psi}} = \frac{K_2 S^2 \left(S + \frac{1}{\tau_2}\right)\left(S + \frac{K_1}{K_2}\right)\left(S + \frac{1}{\tau_7}\right)}{S^3\left(S + \frac{1}{\tau_2}\right)\left(S + \frac{1 - \frac{b_1}{A}}{\tau_7}\right) + \left(\frac{K_5 K_8}{\tau_2}\right)\left(\frac{b_1}{A}\right)\left(S + \frac{1}{\tau_7}\right)\left(S + \frac{K_p}{K_s}\right)\left(S^2 + K_\psi S + K_\psi\right)} \tag{5}$$

The complexity of the equation as a function of A prohibited solving explicitly for A in terms of δ_{I_ψ}. Instead, an iterative procedure was used which consisted of:

1. guessing A

2. calculating the corresponding b_1/A

3. calculating $A = \delta_{I_\psi} \times RHS$

4. comparing calculated A with guess and, if they were not equal, returning to 1.

This iterative procedure was followed until the guessed value of A from step #1 converged upon the calculated value of A from step #3, when the corresponding describing function gain value, b_1/A, for the given system input, δ_{I_ψ}, was able to be found from equation (3). Note equations (3) and (5) show that although the describing function gain is inherently only magnitude dependent, its use in the closed loop analysis causes the limiter input magnitude, A, and hence b_1/A to be frequency dependent also. Thus, the frequency as well as the amplitude component of system input, δ_{I_ψ}, affected the iteration on b_1/A.

It is possible from this relationship to determine the effect on system stability of the amplitude and frequency of the pilots input (δ_{I_ψ}), the servo command limit (a), and the control system bandwidth as determined by the overall system loop gain.

Effect of Implementation on Time Response

In this section, the differences in nonlinear dynamic response between the parallel/series and series servo implementations are illustrated with sample time responses and comparisons of those responses with the theoretical predictions are made as a means of assessing the validity of the theoretical model.

From the discussion in the previous section it may be anticipated that the discernible effect of parallel/series servo implementation is a divergent response once the magnitude of the pilot's input has reached a sufficient level. It may also be anticipated that, although the damping of the series servo mode response is greatly reduced, the response remains stable for all inputs.

Shown in figures 15 through 22 is an experimental comparison between the responses of the parallel/series and series only modes at various input magnitudes and frequencies for the nominal limiter authority of ±.12 inches. Among the time history traces shown are (top to bottom) limiter input, limiter output, yaw acceleration, rate and heading and the pilot's pedal input. Table 1 summarizes the theoretically predicted response (i.e., limiter input magnitude and nonlinear mode frequency and damping) and the results of the experimental comparison at each system configuration.

From figures 15 and 16, it may be seen that the parallel/series system is stable with commanded output, $\dot{\psi}$, in response to each of the low frequency inputs. In figure 15, the low amplitude input of .1 in. does not saturate the limiter. With an input amplitude of .4 in., figure 16 shows the initial response of ψ_{AL} limited to .12 in. with respect to ψ_{BL}; however, the response after this transient remains unsaturated.

Each of these cases was predicted very well by theory as shown in Table 1, the unsaturated responses were predicted by a describing function gain of 1.0 (limiter unsaturated), and no destabilizing nonlinear mode.

The steady state limiter input magnitudes, A or ψ_{BL}, are also corroborated very well.

Increasing the frequency of the low amplitude input to 8 rad/sec in figure 17 shows steady state limiter input, ψ_{BL}, to have increased to .23 in. (compared with a predicted value of .24 in.) and ψ_{AL} as a stable limit cycle. The describing function gain of .56 predicted the introduction of the lightly damped, low frequency mode overlaying the system output, ψ. From the table, the gap between theory and experiment has widened here, with the nonlinear mode predicted to be of higher frequency and higher damping than the experimental results shown. In figure 18, increasing the input amplitude to .4 in. yielded an unstable limit cycle, ψ_{AL}, and a divergent yaw attitude response, ψ, (ζ = -.081). Theory again predicted the initial limiter input accurately, but predicted a higher frequency and more highly damped nonlinear mode ($\zeta \approx 0$).

To summarize the parallel/series configuration response, it was found that an unstable system response may be obtained by increasing either the input amplitude or frequency above a sufficient level. Predictions made using the describing function linearization technique were very accurate when calculating limiter input magnitude; however, the nonlinear mode was consistently less stable than that predicted by theory.

The series servo configuration tolerates a higher limiter input signal before saturation since the limits are proportional to series servo authority (full authority for this configuration). System responses to each of the low frequency inputs, shown in figures 19 and 20, show no saturation and no nonlinear mode overlaying the output. From Table 1 it may be seen that these responses were well predicted by theory. Increasing input frequency to 8 rad/sec in the low amplitude case, figure 21, produces no saturation due to the larger limiter tolerance. (Recall the stable limit cycle in figure 17 for a .1 sin (8t) input into the parallel/series mode.) Again, no destabilizing nonlinear mode is present in the time history, consistent with the theoretical prediction. Increasing the input amplitude to .4 in. (figure 22) produces a stable limit cycle, ψ_{AL}, and a fairly well damped nonlinear mode (ζ = .54). Again, theory predicted a more stable nonlinear mode (ζ = .75) than was found from experiment. Recall that the response of the parallel/series system to an input of .4 sin (8t) (figure 18) was an unstable limit cycle, and divergent aircraft yaw response.

Theoretical predictions of series servo mode response were found to be approximately as accurate as those of the parallel/series mode. In each case limiter input magnitude was predicted very accurately; however, the nonlinear mode damping was overpredicted, indicating a less stable system experimentally than would be anticipated from theory.

In this section, it has been found that the describing function linearization provides a reasonably accurate prediction of system behavior. By substantiating the results of the previous theoretical discussion, it may be concluded that the full authority series configuration, while affected by the low frequency nonlinear mode, will always remain stable. Prediction of the

stability of the parallel/series mode provides the motivation for the balance of this report. Recall that the critical differences in system response between the implementations were due to:

1. a lower limiter input magnitude tolerance in the parallel/series system, and

2. the extra open loop pole at the origin introduced by the parallel/series implementation.

The following sections of the report concentrate: (1) on placing boundaries on the instability in the parallel/series implementation and (2) on evaluating the stabilizing effects of various system configuration changes, keeping in mind the critical differences between the implementations which apparently introduced the instability.

Effect of Input Amplitude and Bandwidth

Addressed in this section of the report is the theoretical prediction of the stability boundary for sinusoidal and square wave inputs, and the accuracy of that prediction, as verified by experiment. Using the iteration technique for describing function gain value as a function of system input discussed previously, the theoretical stability boundary as a function of input amplitude and frequency has been determined. This theoretical boundary is based on the value of b_1/A for neutral stability determined from figure 13. The experimental boundary was found, as shown in the time histories, from the digital model.

Sinusoidal Input.— Figure 23 illustrates the stability boundary for sinusoidal inputs of various magnitudes at the nominal limiter authority of 20% (±.12 inches). The input magnitude which the system will tolerate was found to be inversely proportional to the input frequency. From the figure it can be seen that the theory shows excellent correlation with experimental results for small input amplitudes, and becomes progressively less accurate as the amplitude increases. Recall from the previous comparison of predicted and actual responses that the theory consistently predicted a more stable response than experimental results showed, for the saturated limiter.

Due to the distortion of the frequency response of the nonlinear system between system input magnitude, M, and limiter input magnitude, A, a discontinuity or "jump" resonance, as described in reference 5, was found to exist. Shown in figure 24 is the frequency response of the linear system and the jump discontinuity responses for three nonlinear system input magnitudes. At saturation (recall for nominal 20% series servo authority, the limits are ±.12) for each system input magnitude, M, the limiter input magnitude, A, suddenly jumps to a much higher value causing a sudden decrease in describing function gain, b_1/A, and thus total system gain, sufficient to cause an unstable limit cycle. (Theoretically, this behavior has the characteristics of a hysteresis with the resonance frequency dependent upon the side from

which it is approached, but this was not successfully demonstrated experimentally.) Since the saturation point decreases with input magnitude, the resonance frequency also decreases as a function of input magnitude in a manner consistent with the inverse proportionality between tolerable input magnitude, M, and frequency, ω, shown in figure 23.

This type of insidious instability due to saturation would be extremely hazardous operationally because of its unpredictability to a pilot. Figures 25 and 26 show the time history response which may be anticipated for inputs of $\delta_{I_\psi} = .4\sin(1.22t)$ and $.4\sin(1.25t)$, respectively. The difference between stability and instability in this case was found to be as little as .03 rad/sec. Because the transition to an unstable system is not gradual or predictable, in order to acquire an acceptable pilot-in-the-loop control system, the stability boundary must be avoided during operation or eliminated entirely.

Square Wave Input.— Sudden maneuvers require more abrupt pilot inputs and are better approximated by a square wave. In this section of the report, the magnitude vs. frequency stability boundary established in the previous discussions has been extended to include a square wave. Using Fourier series, as described in reference 6, the square wave has been modeled analytically by equation (6) using up to the 21st harmonic of the fundamental frequency component.

$$\delta_{I_\psi} = \frac{M}{\pi} \sum_{n=1}^{21} \frac{1}{n} \sin n t \qquad (6)$$

A theoretical model including the complexity of the 21st harmonic was chosen because of the very close resemblance of the time response using this representation and that of a square wave as shown in figures 27 and 28. In figure 28, upstream signals, ψ_{BL}, ψ_{AL}, and yaw acceleration, $\ddot{\psi}$, include a significant amount of the higher frequency Fourier series components. However yaw attitude response, ψ, is virtually identical to that commanded by the actual square wave, as in figure 27.

System stability for a sine wave input was found to be very sensitive to input frequency. It would be anticipated that, because of the composition of very high frequencies required to model the straight sides of the square wave, system stability to a square wave input would be reduced significantly from that of a sine wave.

Shown in figure 29 are the theoretical and experimental stability boundaries for a square wave system input. The theoretical curve was generated using the Fourier series approximation as the input into the iteration technique for describing function gain value. The experimental curve reflects system response to an actual square wave, rather than the Fourier series approximation. As shown, the stability boundary is reduced significantly from the sinusoidal case in each magnitude and frequency. For example, a square wave input of amplitude $M/M_{max} = .1$ becomes unstable at .15 rad/sec as compared with 1.8 rad/sec for a sinusoidal input of the same amplitude. As with the sinusoidal stability boundary, for higher input magnitudes, theory

predicts a more stable response than the experimental results show. Jump resonance phenomena also exist here, as shown in the distorted frequency response of system input magnitude to limiter input magnitude in figure 30. Due to the multi-frequency composition of the square wave, several jump discontinuities exist at different resonance frequencies.

Thus, the magnitude-frequency boundary is also a function of input shape; specifically, stability of the system response is significantly more sensitive to a square wave than to a sinusoidal input.

Effect of Series Servo Authority

One of the critical differences between the parallel/series and series servo systems is the higher limiter values of the latter which occur because of the proportionality between series servo authority and limiter magnitude. Nominal limits of the parallel/series system are based on 20% series servo authority and the maximum practical limits would be based on 50%. In this section of the report, the effect of variation of series servo limits on the nonlinear system has been evaluated.

Theoretically, the result of increased series servo authority may be understood to have a stabilizing effect on system response by recalling the dependence of describing function gain, b_1/A, on limiter size, a, from equation (3). As the limiter magnitude is increased, so is the minimum allowable describing function gain value, yielding greater system stability.

From figure 31 (generated analytically) it may be seen that the stability boundary as a function of series servo authority normalized to input magnitude varies almost linearly with low sinusoidal input frequencies. As the ratio of series servo authority to input magnitude increases (either by increasing series servo authority or decreasing input magnitude, as previously discussed) the system's tolerance to input frequency is increased. Note that a percentage of series servo authority normalized to input magnitude exists such that at or above which the system has a stable response at all input frequencies.

The trend toward increased system stability for increased series servo authority is further illustrated in figure 32. The comparison of magnitude-frequency tradeoff for nominal and increased series servo authority, 20% and 50%, respectively, was found to show a significant increase in the stability boundary at the maximum practical limit of 50% series servo authority.

Effect of System Bandwidth

Evaluated in this part of the report are the influences of system bandwidth on nonlinear system stability. Contributions to bandwidth that are considered are the yaw angle and rate feedback gains and the parallel servo gain in the forward loop.

Yaw Angle and Rate Feedback Gain Variations.— Variation of the yaw angle feedback gain, K_ψ (as in figure 4), with simultaneous variation of the yaw rate feedback gain, $K_{\dot{\psi}}$, in order to maintain adequate closed loop damping, showed a significant increase in linear system phase margin but almost no change in gain margin. This is illustrated in figure 33 for variations in K_ψ and $K_{\dot{\psi}}$ from the nominal values of 4.0 and 4.0 to .5 and 1.45, respectively.

However, nonlinear stability boundary changes were found to be unfavorable for reduction of yaw angle and rate feedback gains as shown in figure 34. From the figure, two trends were noted: (1) as system bandwidth was reduced, the system's tolerance to magnitude at high input frequencies was increased slightly because of the lower describing function gain value for neutral stability due to the lower feedback gains, K_ψ and $K_{\dot{\psi}}$. However (2), for the same amount of system bandwidth reduction, a much greater reduction in input bandwidth occurred. Equation (5) shows the relationship between system input, δ_{I_ψ}, describing function gain, b_1/A, and the yaw angle and rate feedback gains, K_ψ and $K_{\dot{\psi}}$.

More favorable nonlinear system results were obtained by varying only the yaw angle feedback gain, while maintaining the yaw rate feedback gain at its nominal value. (This resulted in a 20% to 30% decrease in closed loop damping ratio.) Varying K_ψ showed little effect on linear system stability criteria, as illustrated in figure 35 for values of K_ψ from the nominal value of 4.0 to the limiting value of 0.

Changes in the nonlinear system stability boundary with K_ψ were found to exhibit the same two general trends as previously noted (figure 36). Specifically, these were a reduction in tolerable input bandwidth and an increased level of system tolerance to magnitude at high input frequencies. In this case, however, the increased tolerance to magnitude at high frequencies outweighs the input bandwidth loss, resulting in a net favorable effect on the nonlinear stability boundary.

Recall that a critical difference between the parallel/series and series only systems was the introduction of an open loop pole at the origin into the parallel/series system by the parallel servo. This extra open loop integrator had a destabilizing influence on the parallel/series system as was shown in figures 13 and 14. Elimination of the yaw angle feedback ($K_\psi = 0$) changed the parallel/series system into one with only three open loop poles at the origin (as in the series only system).

Figure 37 illustrates the variation of the system eigenvalues with describing function gain value for the closed loop system without yaw angle feedback. From the figure it may be seen that as the describing function gain, b_1/A, approaches zero, the branches of closed loop eigenvalues depart vertically and remain in the left half plane. In figure 36, then, the stability boundary is completely eliminated for $K_\psi = 0$. Stabilizing the system in this manner does not preclude the existence of the low frequency nonlinear mode. The frequency and damping of this mode vary, as before, with describing function gain value, calculated from equation (5) as a function of system

input. Eliminating the yaw angle feedback and thereby stabilizing the system ensures only that the damping of this mode will be positive.

Yaw angle feedback elimination changes the system from the designed rate-command-attitude-hold configuration to rate-command only. System response, although stable for all inputs, lacks directional-hold capability. With an inadequate yaw rate sensor, heading drift may present a problem; also, removal of attitude-hold removes the control system's resilience to wind or turbulence upsets.

Parallel Servo Gain Variations.— In terms of operational safety considerations, it was desirable to maximize the saturation time following a runaway failure, and thus minimize parallel servo gain, K_{p_s}. Another consideration in gain selection was the upstream limiting of the parallel servo input signal by the series servo limiter. Due to the proportionality of the series servo limiter value to series servo authority, the parallel servo gain was chosen to be inversely proportional to this parameter. Parallel servo gain, then, as shown in equation (7) is a function of the time which is allowed for saturation of the parallel servo in the case of a runaway failure and of the fraction of the total control power allotted to the series servo.

$$K_{\substack{\text{parallel} \\ \text{servo}}} = \frac{1}{\left(\begin{matrix}\text{Series Servo} \\ \text{Authority}\end{matrix}\right)\left(\begin{matrix}\text{Saturation} \\ \text{Time}\end{matrix}\right)} \tag{7}$$

The same trends as in the previous discussion were apparent with the system bandwidth reduction due to lowering of the parallel servo gain, K_{ps}. Linear system phase and gain margins were found to increase, although much more significantly than in the case of the attitude feedback gain, with parallel servo gain reduction, as illustrated in figure 38. From the figure, it may be seen that a significant stabilization of the linear system occurs with reduced parallel servo gain.

With the nominal value of 20% series servo authority, the minimum value of parallel servo gain may be established to be $K_{ps} = .25$, based on a maximum practical saturation time of 20 seconds. If the series servo authority were increased to the maximum reasonable level of 50%, a minimum value of $K_{ps} = .1$ is acceptable. The same general trends, specifically a reduction in tolerable input bandwidth and an increased level of system tolerance to magnitude at high input frequencies as were previously noted for attitude feedback gain reduction, were found to also apply to the reduction of parallel servo gain. These trends are illustrated for the nonlinear system with 20% series servo authority in figure 39 where it may be seen that the undesirable loss of input bandwidth far outweighs the gain in system tolerance to magnitude at high frequencies for a given reduction in parallel servo gain. Figure 40 shows the change in nonlinear stability boundary with parallel servo gain for a system with 50% series servo authority. The combination of the inherently stabilizing effect of increased servo authority and the smaller minimum acceptable parallel servo gain of $K_{ps} = .1$ resulted in a net favorable effect on the nonlinear stability boundary.

CONCLUSIONS

The analysis described in this report encompassed linear and nonlinear stability analyses of the state-rate-feedback-implicit-model-following control system of reference 3. Theoretical stability predictions of the nonlinear system were accomplished using a describing function linearization technique. Experimental results obtained from a digital model were used to substantiate the theory. From this analysis, the following specific conclusions have been drawn:

1. The experimental analysis using the simplified Fortran model was accomplished non-real-time with a sampling period of T = .005 seconds. Although the real-time computer simulation uses a sampling period of T = .05 seconds, the linear system's dynamic characteristics were found to be represented much more accurately with T = .005 seconds.

2. Analytical prediction of nonlinear system stability using the describing function linearization technique for a simple limiter was found to be valid for each of the sinusoidal and square wave system inputs.

3. In its nominal configuration, the full authority series servo mode was found to be stable at all system inputs; the parallel/series servo mode was found to be conditionally stable and possibly unacceptable for inputs which saturate the limiter upstream of the parallel and series servos. This conditional stability results from the extra open loop pole at the origin introduced in the parallel/series implementation. The effect of the series servo position limiter is sufficient to reduce the system gain and introduce a low frequency instability.

4. A stability boundary, in which tolerable input magnitude was inversely proportional to input frequency was found to exist in the parallel/series servo mode. In terms of this stability boundary, significantly more sensitivity was observed to a square wave input due to its high frequency composition than to a sine wave input.

5. Increasing the fraction of total control power allotted to the series servo was found to have a significantly favorable effect on the stability of the nonlinear system with parallel/series servo implementation. Increasing the series servo authority to its maximum practical level was found to raise, but not eliminate, the stability boundary.

6. In terms of the magnitude-frequency stability boundary, reduction of yaw angle and rate feedback gains was found to affect the nonlinear stability boundary unfavorably. Yaw angle feedback gain reduction (alone) improved stability, resulting in a relatively small input bandwidth reduction and a more significant increase in system tolerance to magnitude at high input frequencies. Elimination of yaw angle feedback was found to stabilize the parallel/series system; however removal of the attitude hold capability reduces the system's resilience to rate gyro drift or atmospheric disturbances.

7. Parallel servo gain reduction (alone) was found to have an adverse effect on nonlinear system stability. The small increase in system tolerance to magnitude at high input frequencies was by far outweighed by the relatively large loss of input bandwidth. The combination of parallel servo gain reduction and series servo authority increase was found to improve nonlinear system stability.

REFERENCES

1. Radford, R. C.; and Andrisani, D.: An Experimental Investigation of VTOL Flying Qualities Requirements in Shipboard Landings. AIAA Paper No. 80-1625-CP, August 1980.

2. Corliss, L. D.; Greif, R. K.; and Gerdes, R. M.: "Comparison of Ground-Based and In-Flight Simulation of VTOL Hover Control Concepts," Journal of Guidance and Control, Vol. 1, No. 3, May-June 1978, pp. 217-221.

3. Merrick, V. K.: Study of the Application of an Implicit Model-Following Flight Controller to Lift Fan VTOL Aircraft. NASA TP-1040, 1977.

4. Hall, J. R.; and Bennett, Lt. P. J.: The Ability of a Safety Pilot to Recover a Jet V/STOL Aircraft Following Control Runaways in Hover: A Simulator Study. RAE TR-80033, March 1980.

5. Graham, D.; and McRuer, D.: Analysis of Nonlinear Control Systems. John Wiley and Sons, Inc. 1961.

6. Clement, P. R.; and Johnson, W. C.: Electrical Engineering Science. McGraw-Hill Book Company, Inc., 1960.

APPENDIX

GAIN EQUIVALENCES AND INITIAL VALUES

SRFIMF	Initial Numerical Value
$LM_{\delta I_\psi}$	±2.1 in.
K_{10}	0.3948
K_{20}	0.9349
K_ψ	4.0
$K_{\dot{\psi}}$	4.0
K_{ψ_H}	0.3324
LM_{ψ_C}	±0.12 in.
τ_7	0.05/sec
K_{30}	2.533
G_Y	1.0
K_{Y_C}	1.0
FCN	7.5

Analysis	SRFIMF	Initial Numerical Value
δI_ψ	δI_ψ	--
$LM\delta I_\psi$	$LM_{\delta I_\psi}$	±2.1 in.
K_1	$(K_\psi \times K_{\psi_H})$	1.33
K_2	$(K_{10} + K_{20})$	1.33
K_3	$(K_{30} \times G_Y \times FCN \times K_{TORQUE}/I_z)$	0.7082
K_5	(K_{TORQUE}/I_z)	0.0373
K_{ps}	--	2.5
K_p	$(K_{30} \times K_{ps} \times K_{Y_C} \times FCN)$	47.49
K_{ss}	--	7.0
K_s	$(K_{ss} \times K_{30})$	17.73
K_ψ	K_ψ	4.0
$K_{\dot{\psi}}$	$K_{\dot{\psi}}$	4.0

Analysis	SRFIMF	Initial Numerical Value
$\pm a$	$\pm LM_{\psi_C}$	± 0.12 in.
τ_7	τ_7	0.05/sec
τ_2	--	0.10/sec
K_{TORQUE}	--	1200 deg-lb_f
I_z	I_z	32192 slug-ft^2

TABLE 1.- COMPARISON OF THEORETICALLY PREDICTED AND EXPERIMENTAL SYSTEM RESPONSE: NOMINAL 20% SERIES SERVO AUTHORITY, a = ±0.12.

INPUT, δ_{I_ψ}		PARALLEL/SERIES SERVO CONFIGURATION				SERIES SERVO CONFIGURATION			
		Describing Function Gain, b_1/A	Limiter Input Magnitude, $A{:}\psi_{BL}$	Nonlinear Mode Frequency, rad/sec	Nonlinear Mode Damping	Describing Function Gain, b_1/A	Limiter Input Magnitude, $A{:}\psi_{BL}$	Nonlinear Mode Frequency, rad/sec	Nonlinear Mode Damping
0.1 sin (1t)	THEORY	1.0	0.0199	N/A	N/A	1.0	0.054	N/A	N/A
	EXP'MT		0.021				0.055		
0.4 sin (1t)	THEORY	1.0	0.0798	N/A	N/A	1.0	0.215	N/A	N/A
	EXP'MT		0.08				0.21		
0.1 sin (8t)	THEORY	0.56	0.24	2.27	0.35	1.0	0.32	N/A	N/A
	EXP'MT		0.23	1.9	0.25		0.33		
0.4 sin (8t)	THEORY	0.216	0.649	1.50	~0	0.703	0.935	1.050	0.75
	EXP'MT		0.7	1.28	-0.081		0.95	1.047	0.54

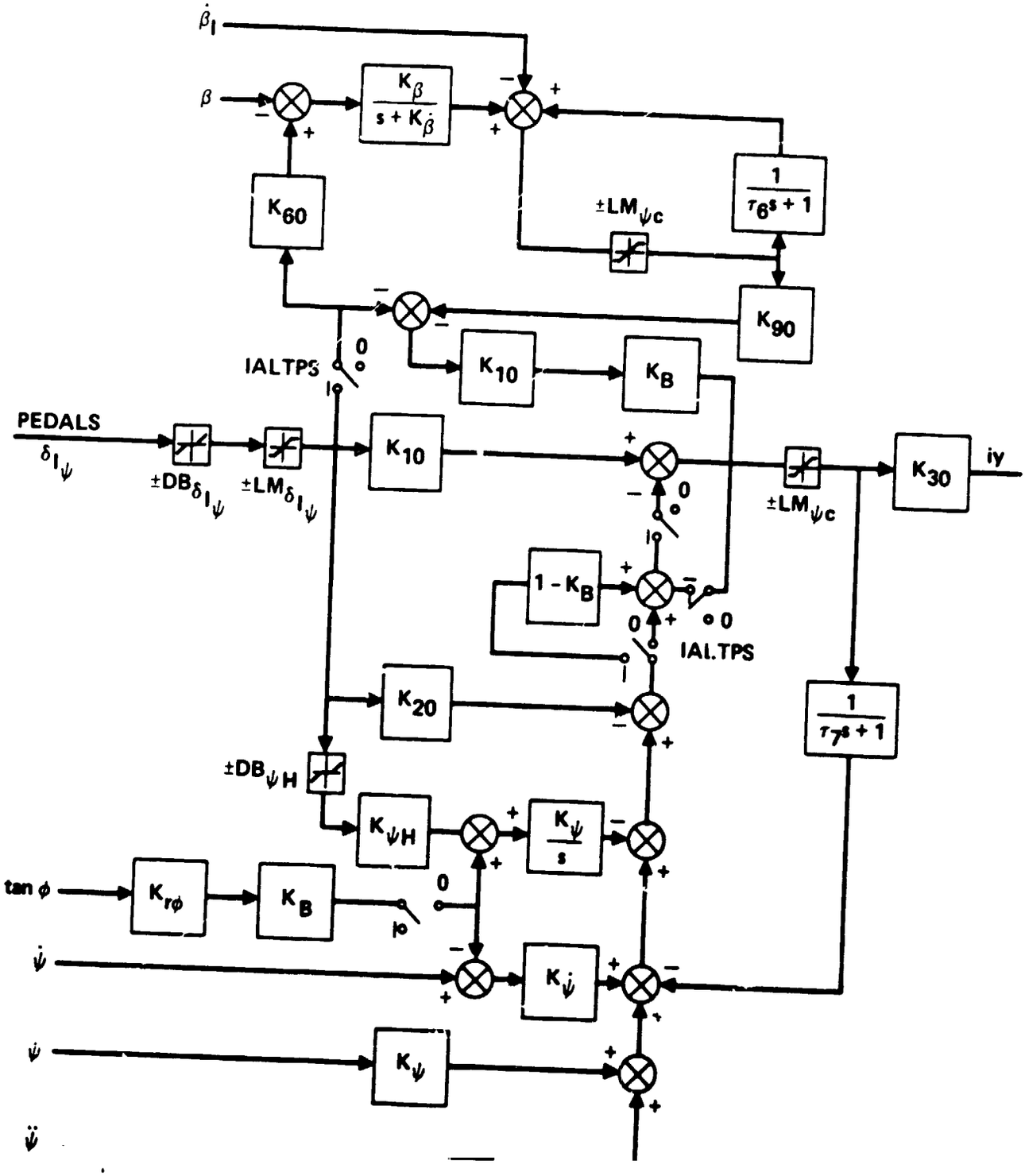

Figure 1.- State rate feedback implicit model following control system.

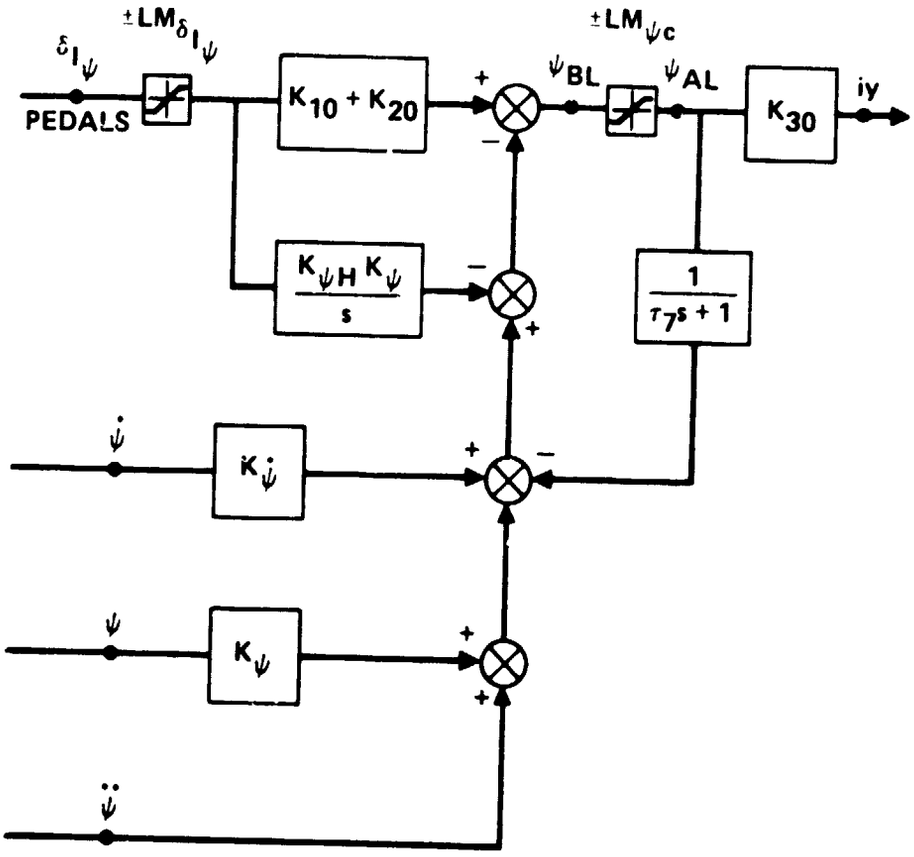

Figure 2.- Simplified yaw control system.

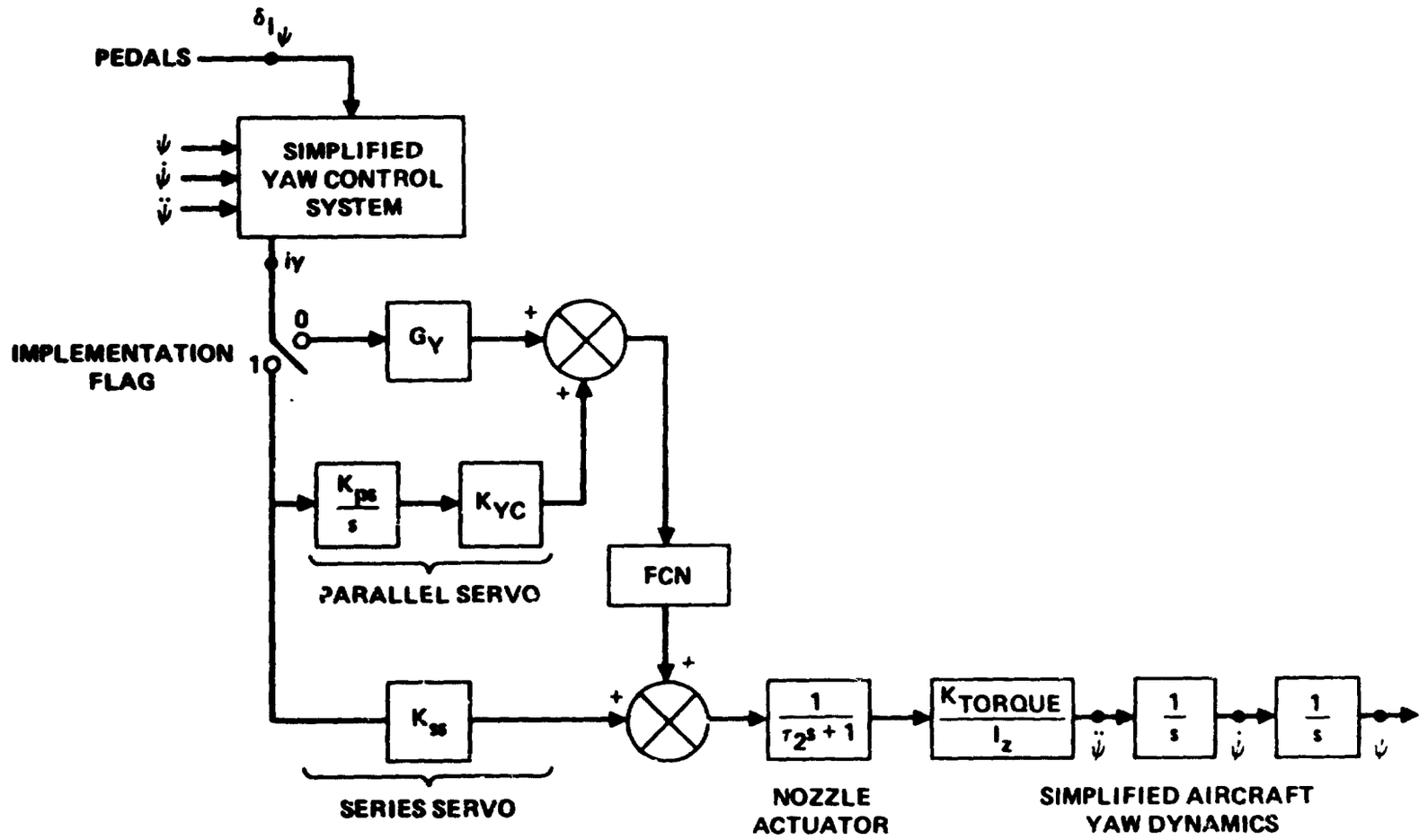

Figure 3.- Simplified yaw control system, mechanization and actuation dynamics.

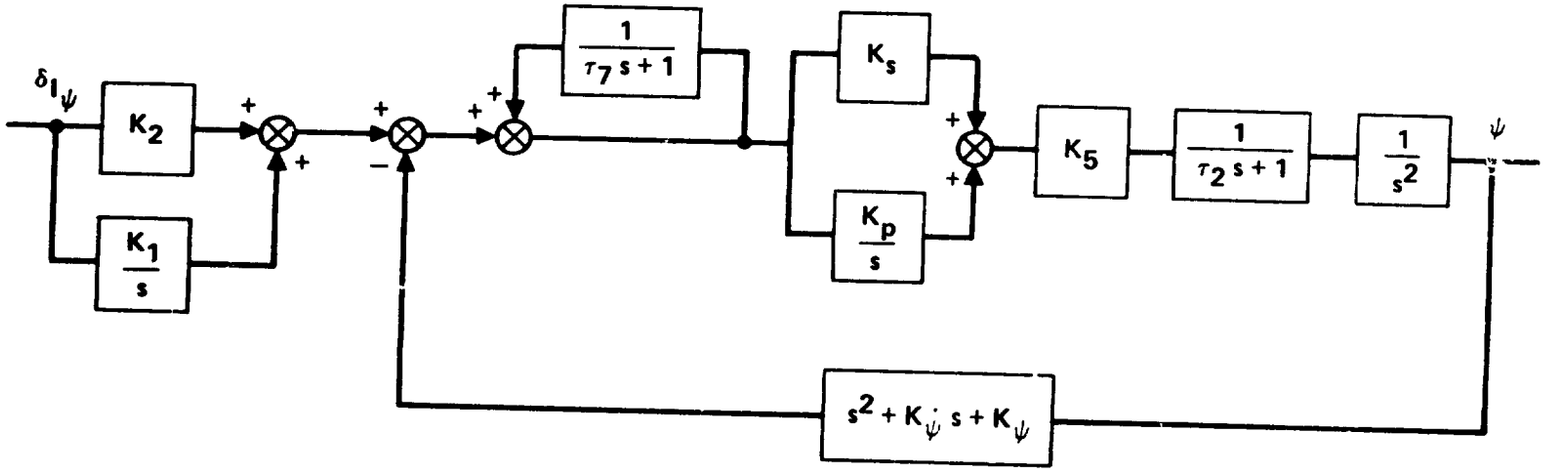

Figure 4.- Linear simplified model: parallel/series servo mode.

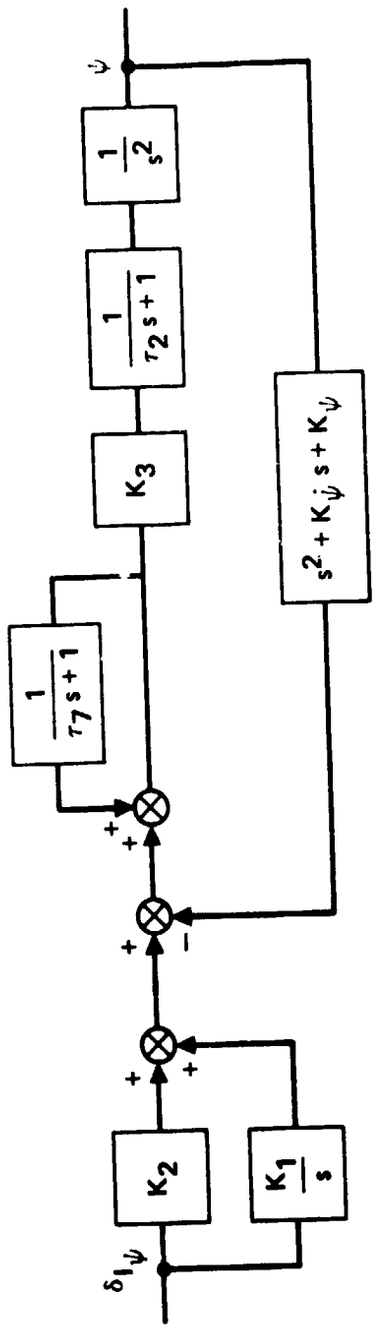

Figure 5.- Linear simplified model: series servo mode.

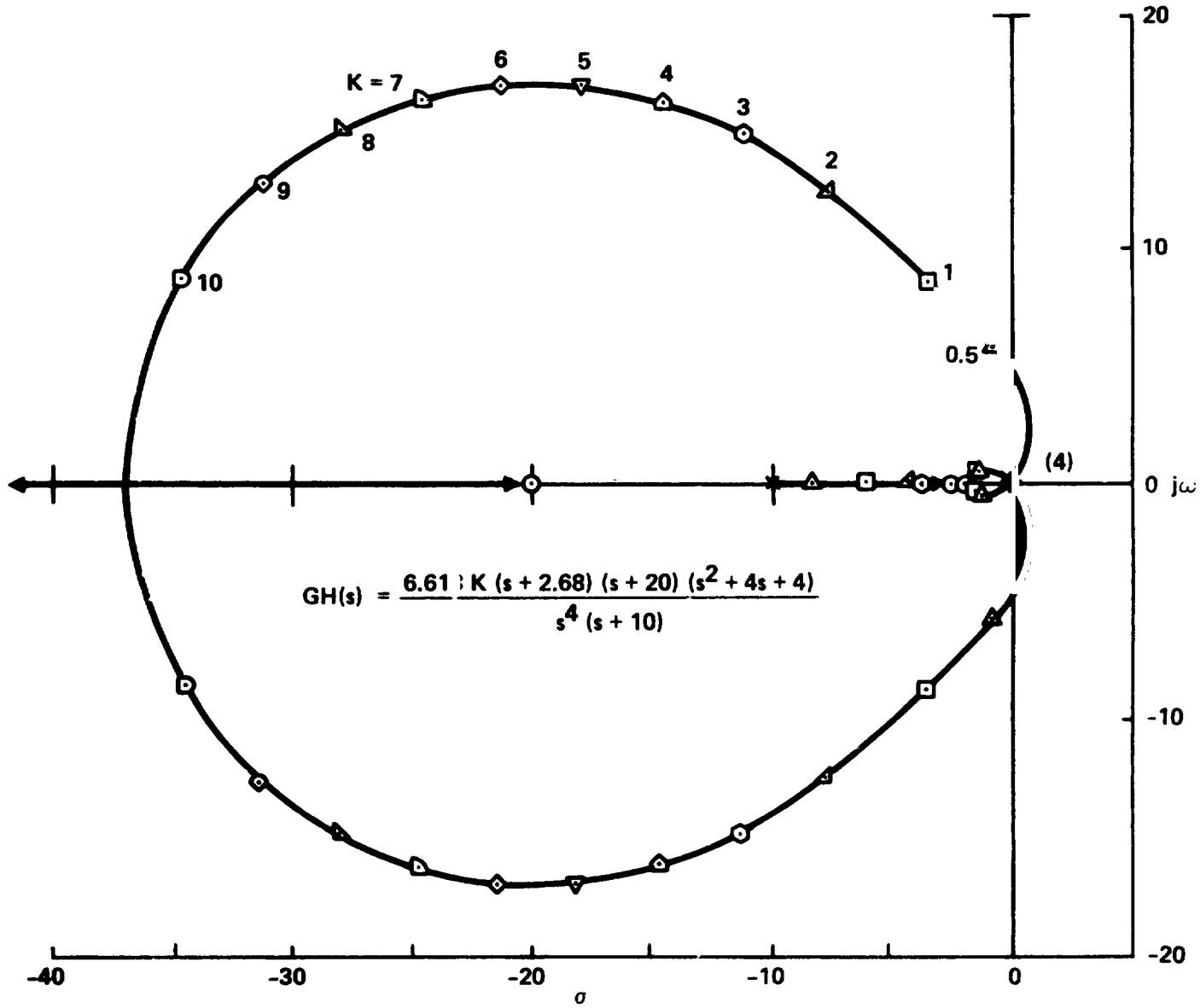

Figure 6.- Root locus of linear system, parallel/series servo mode.

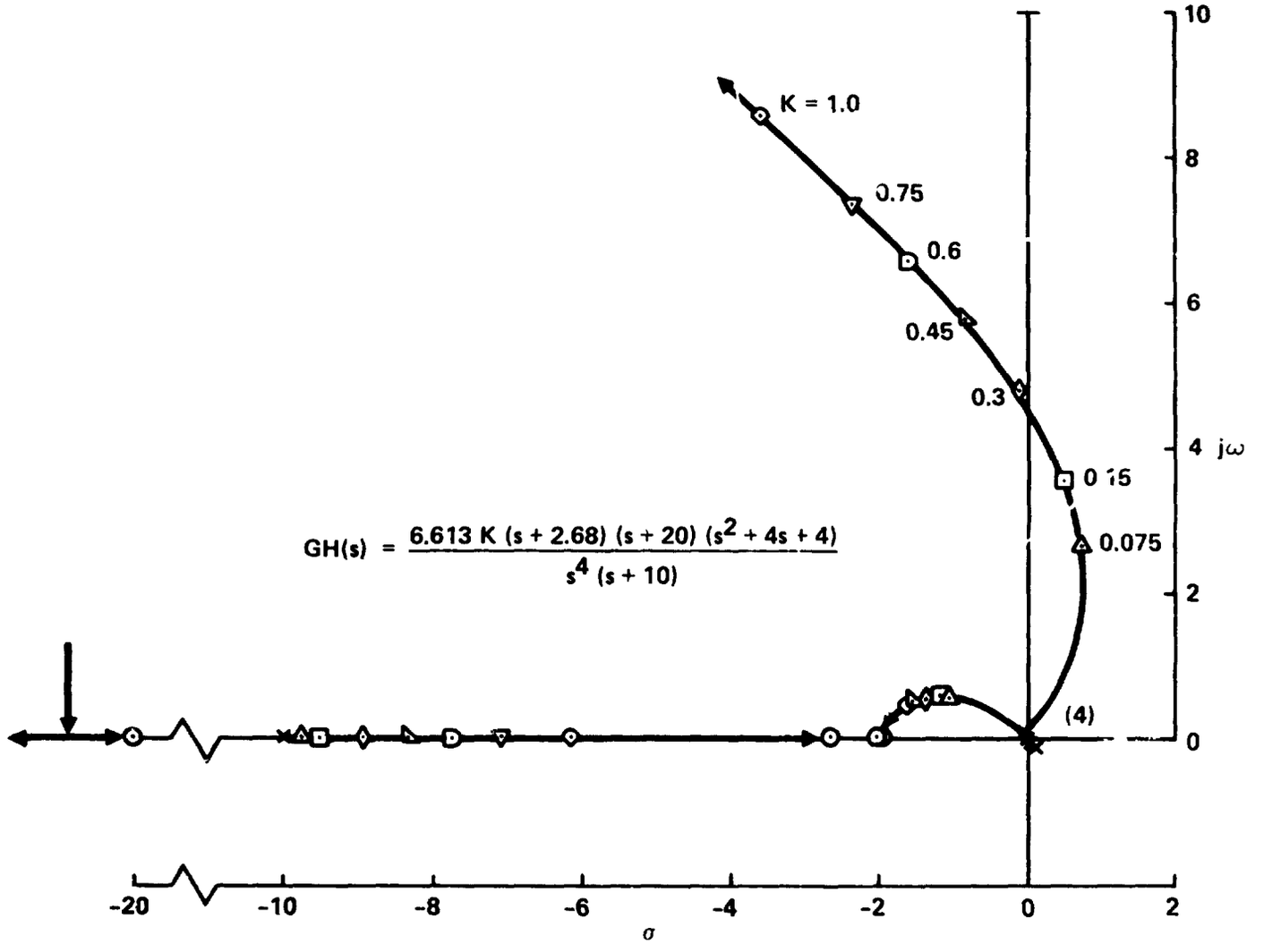

Figure 7.- Partial root locus of linear system, parallel/series servo mode.

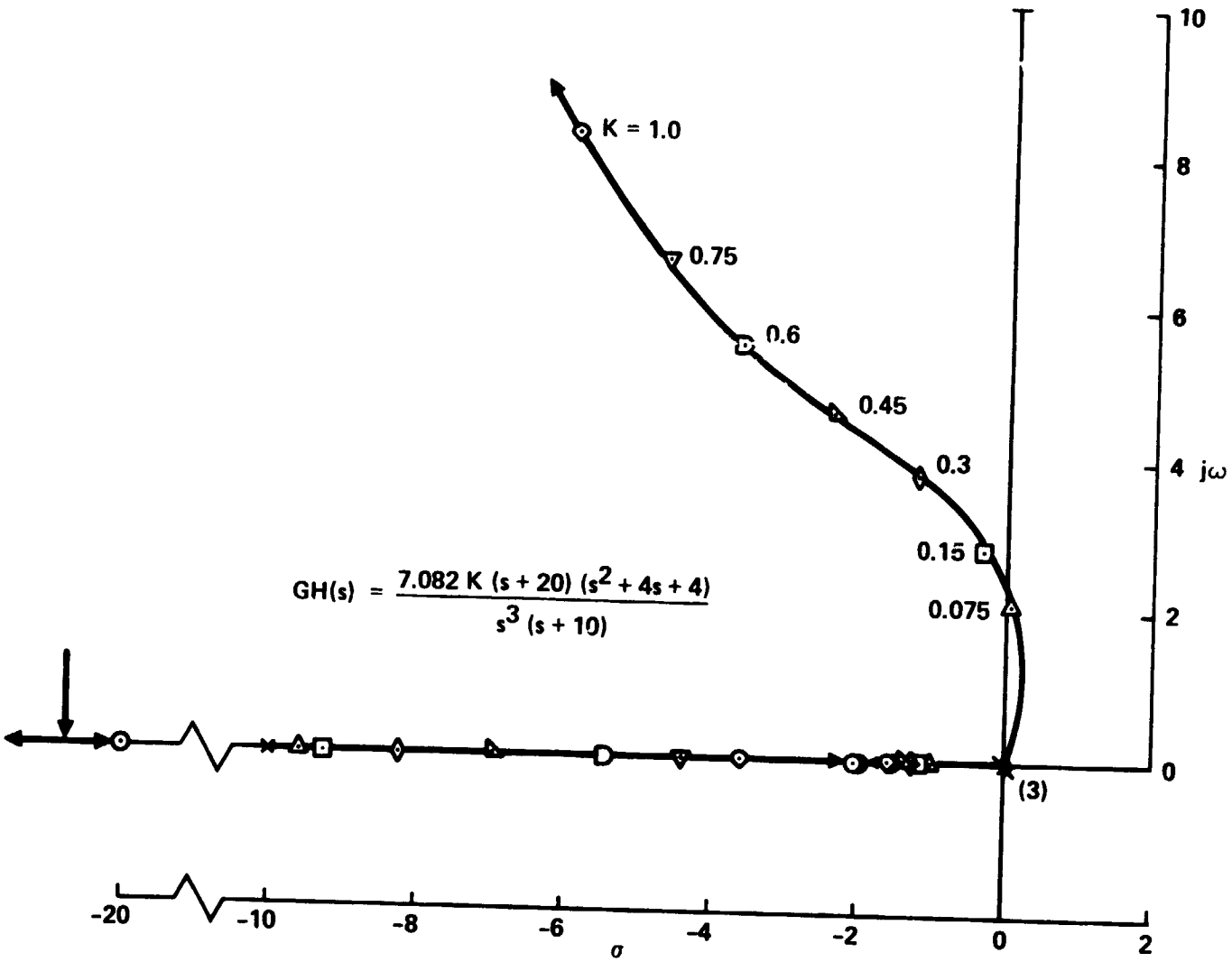

Figure 8.- Partial root locus of linear system, series servo mode.

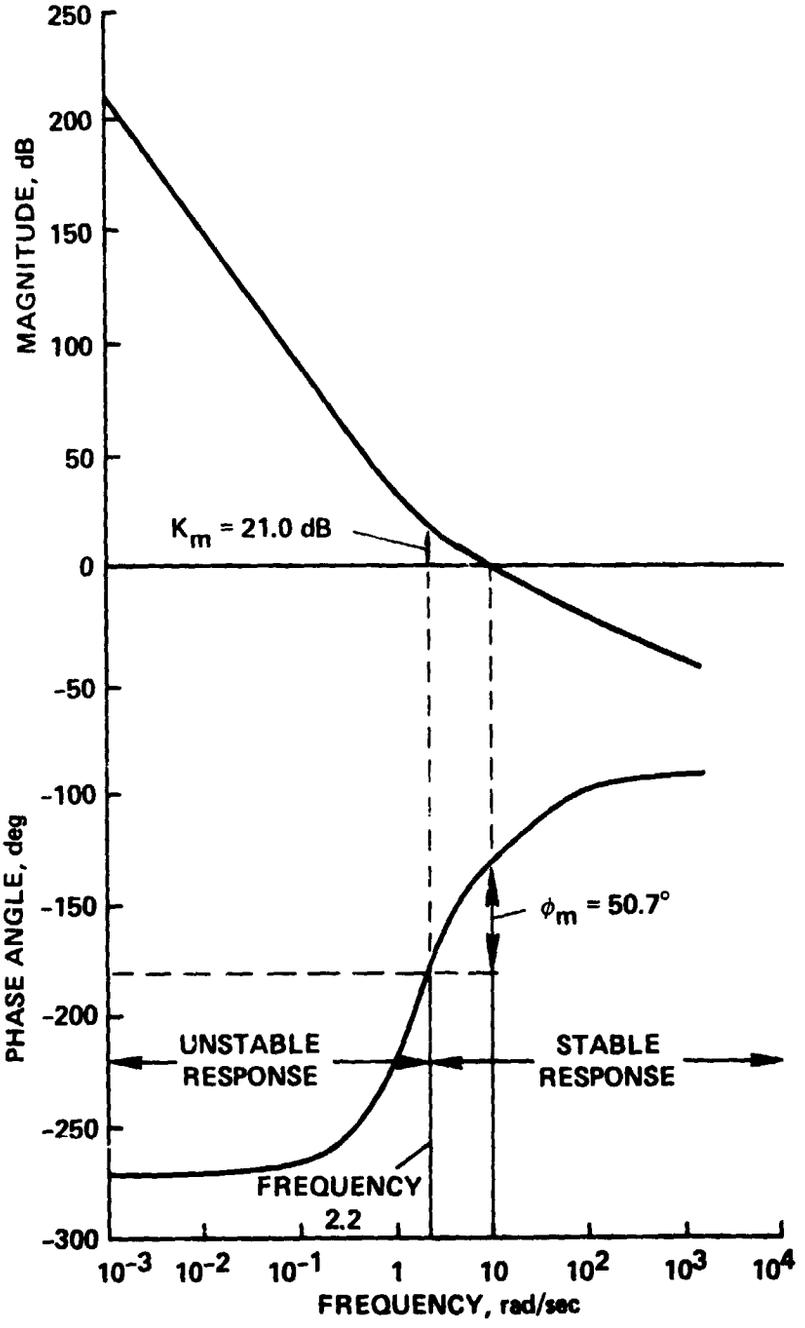

Figure 9.- Frequency response of linear system, series servo mode.

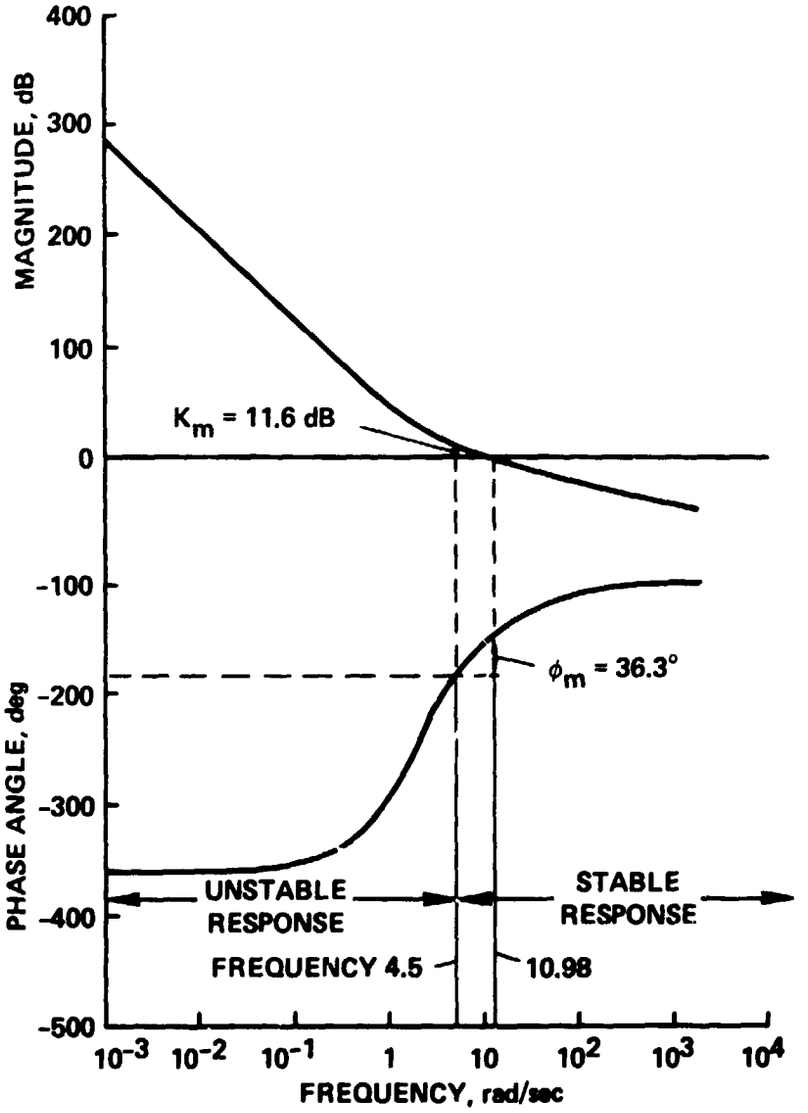

Figure 10.- Frequency response of linear system, parallel/series servo mode.

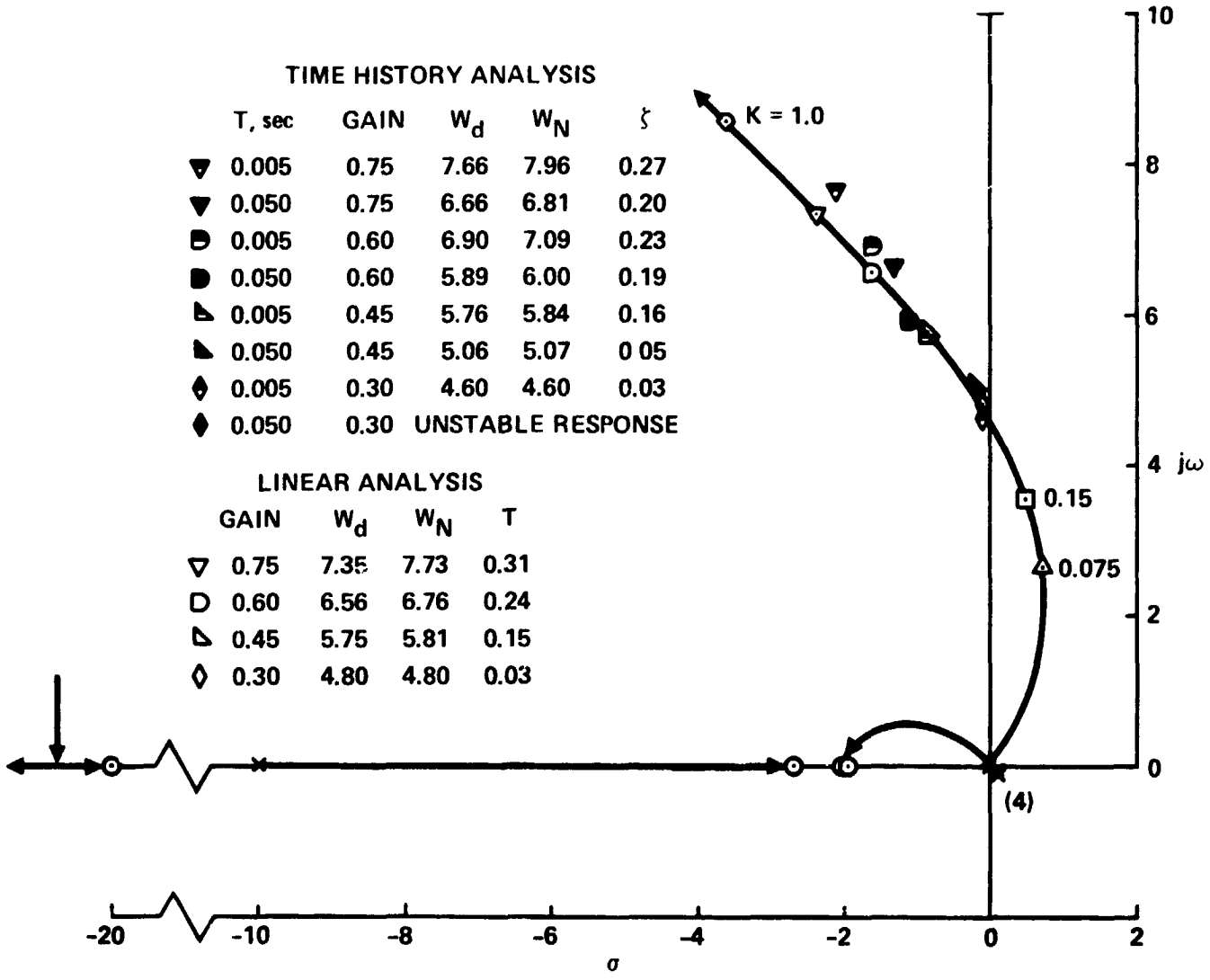

Figure 11.- Time history vs. linear analysis, parallel/series servo mode.

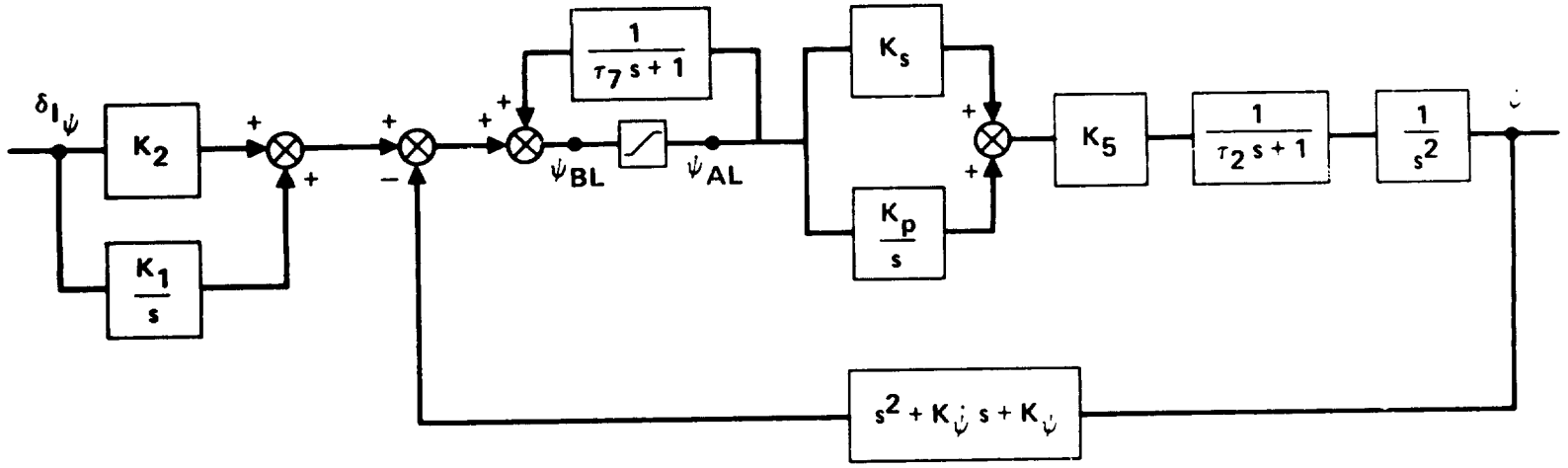

Figure 12.- Nonlinear simplified model: parallel/series servo mode.

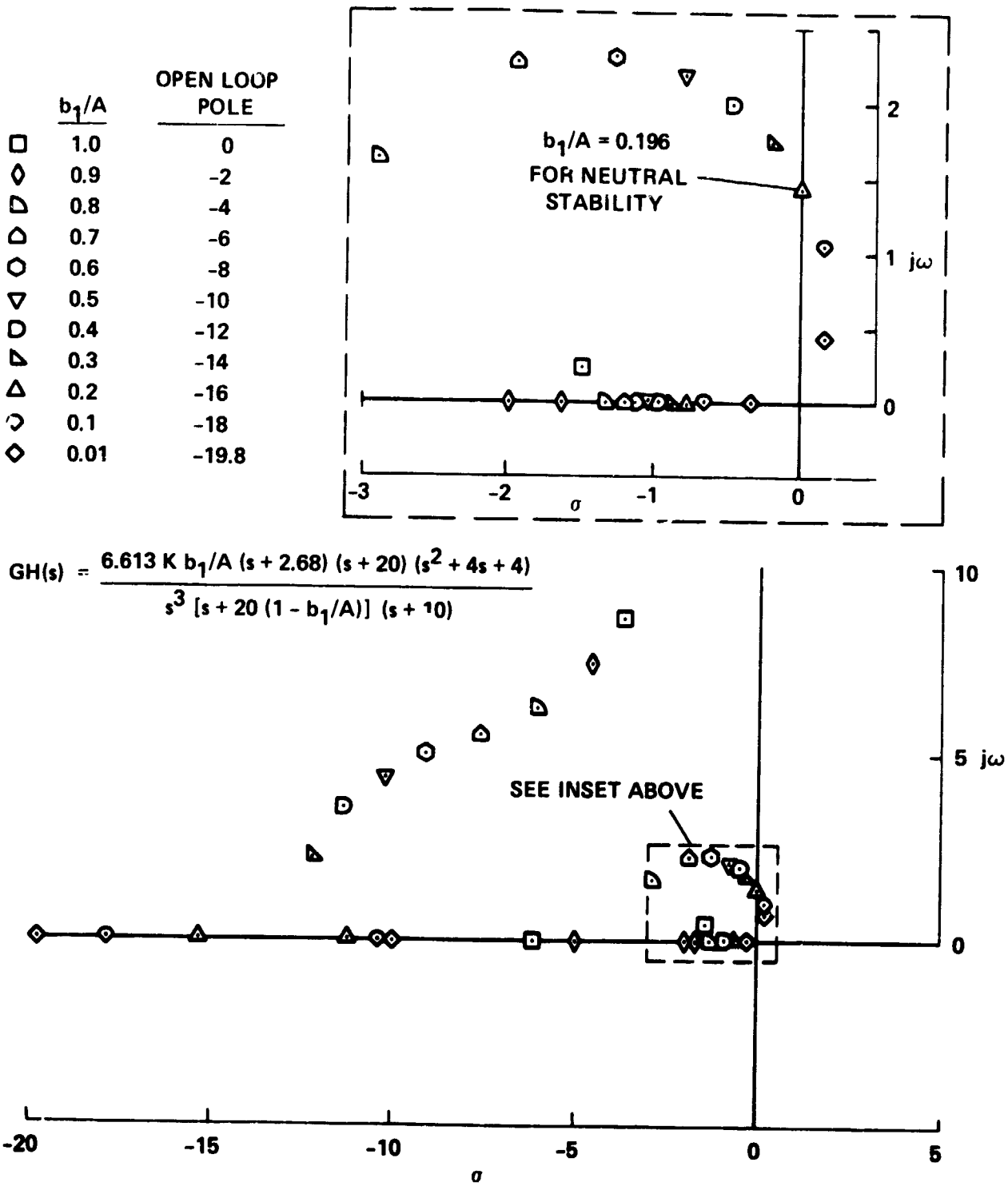

Figure 13.- Variation of closed-loop roots with magnitude of nonlinearity (b_1/A), parallel/series servo mode.

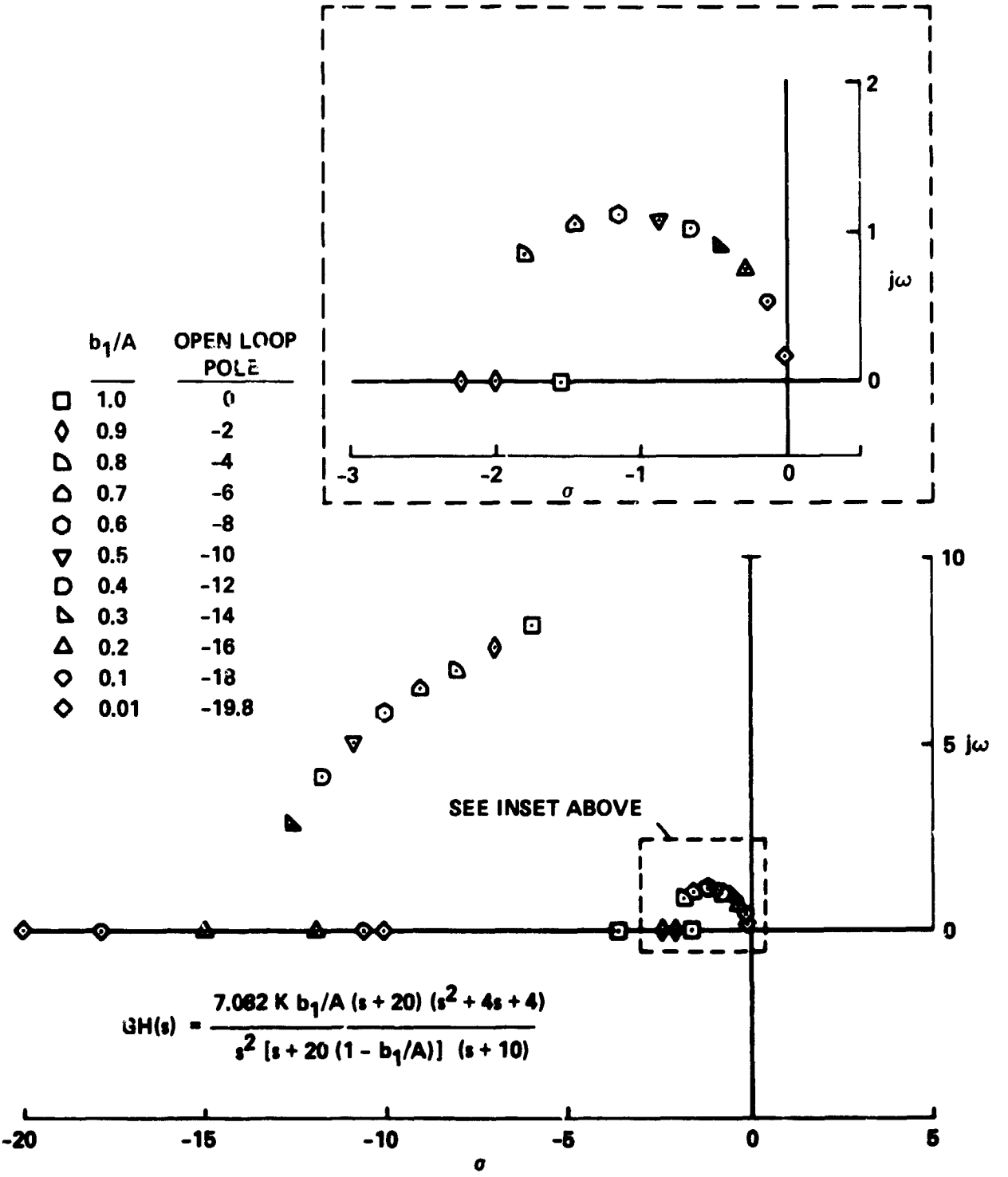

Figure 14.- Variation of closed-loop roots with magnitude of nonlinearity (b_1/A), series servo mode.

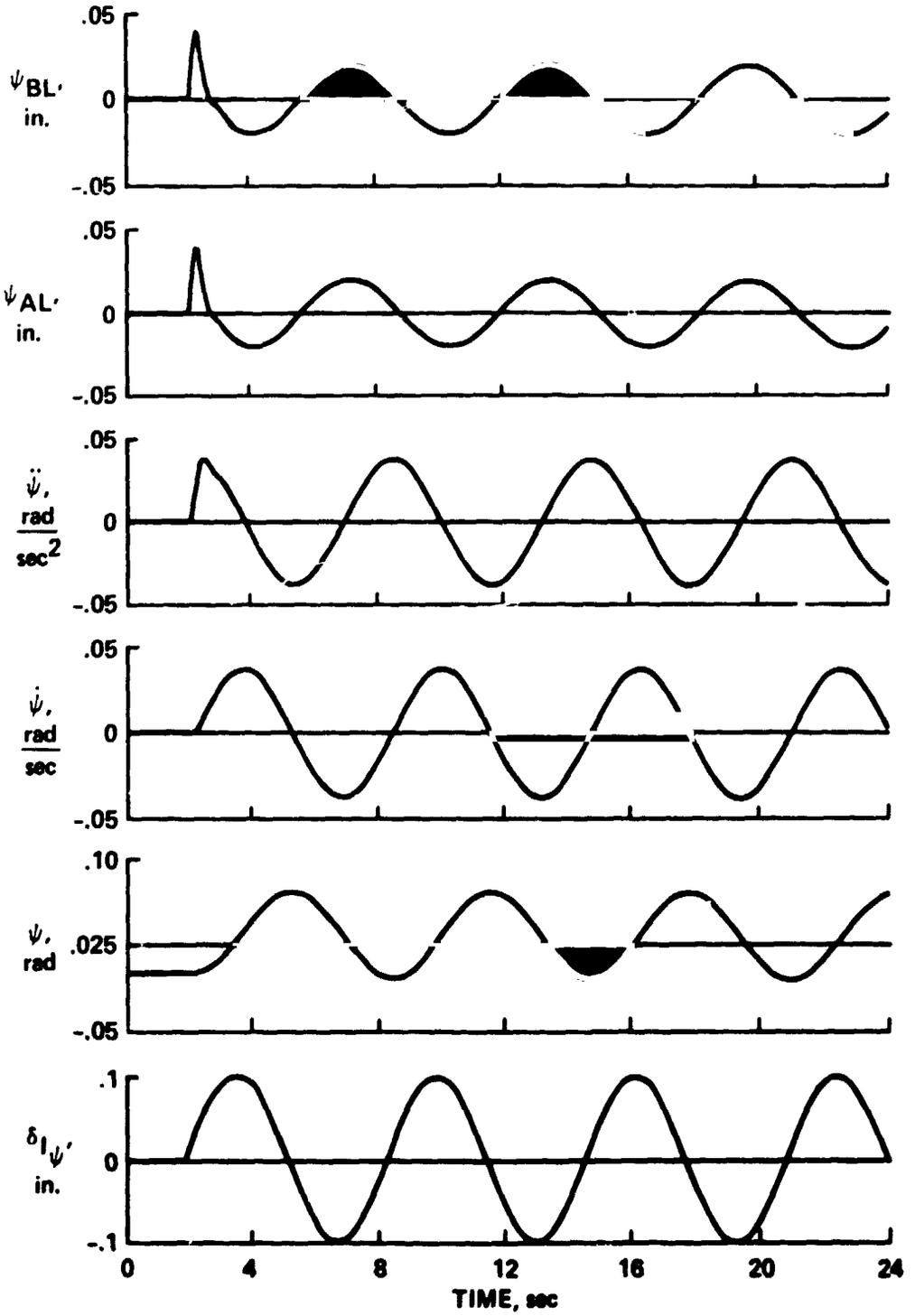

Figure 15.- Nominal configuration, parallel/series servo, δ_{I_ψ} = 0.1 sin (1.0t).

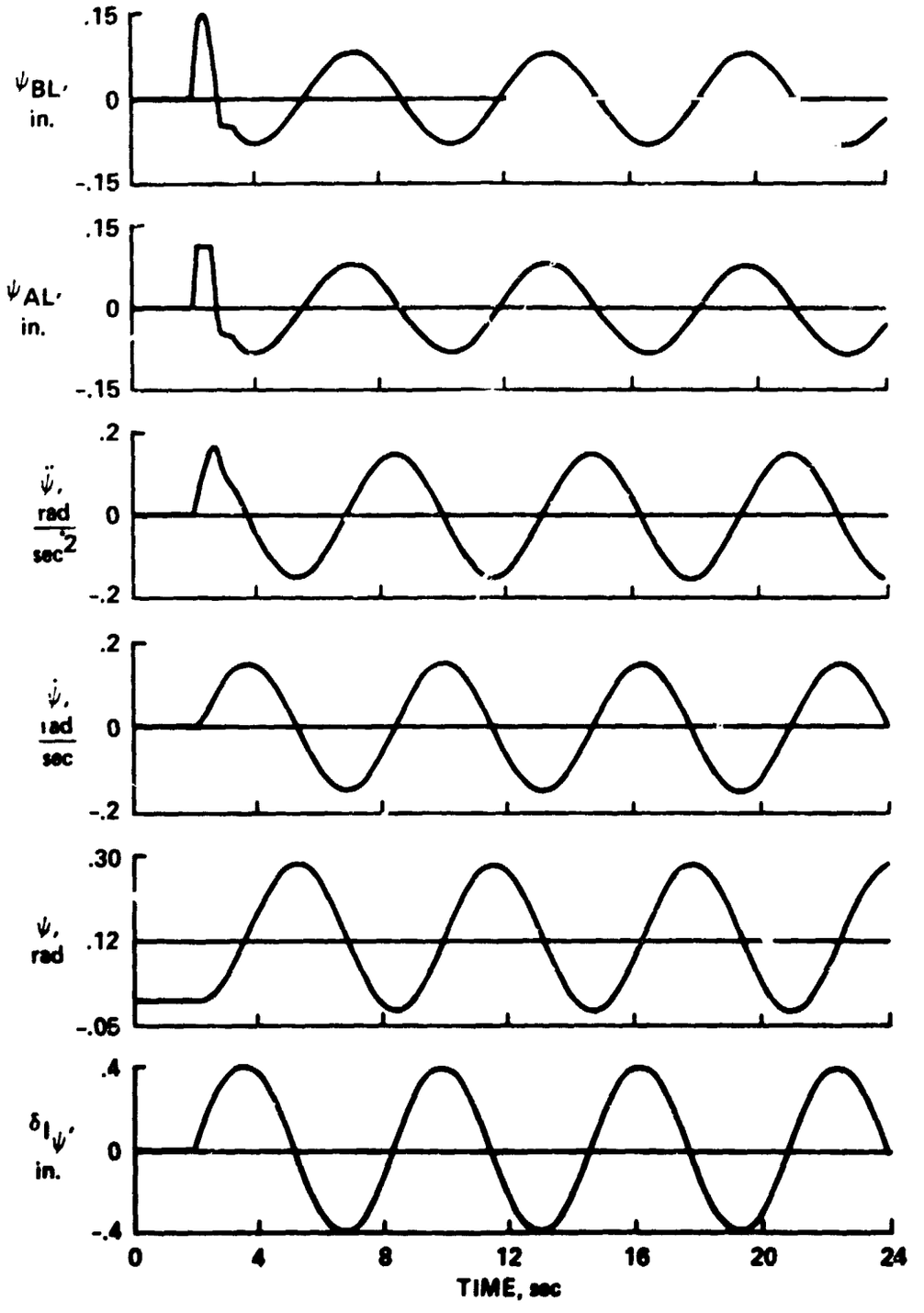

Figure 16.- Nominal configuration, parallel/series servo, $\delta_{I_\psi} = 0.4 \sin (1.0t)$.

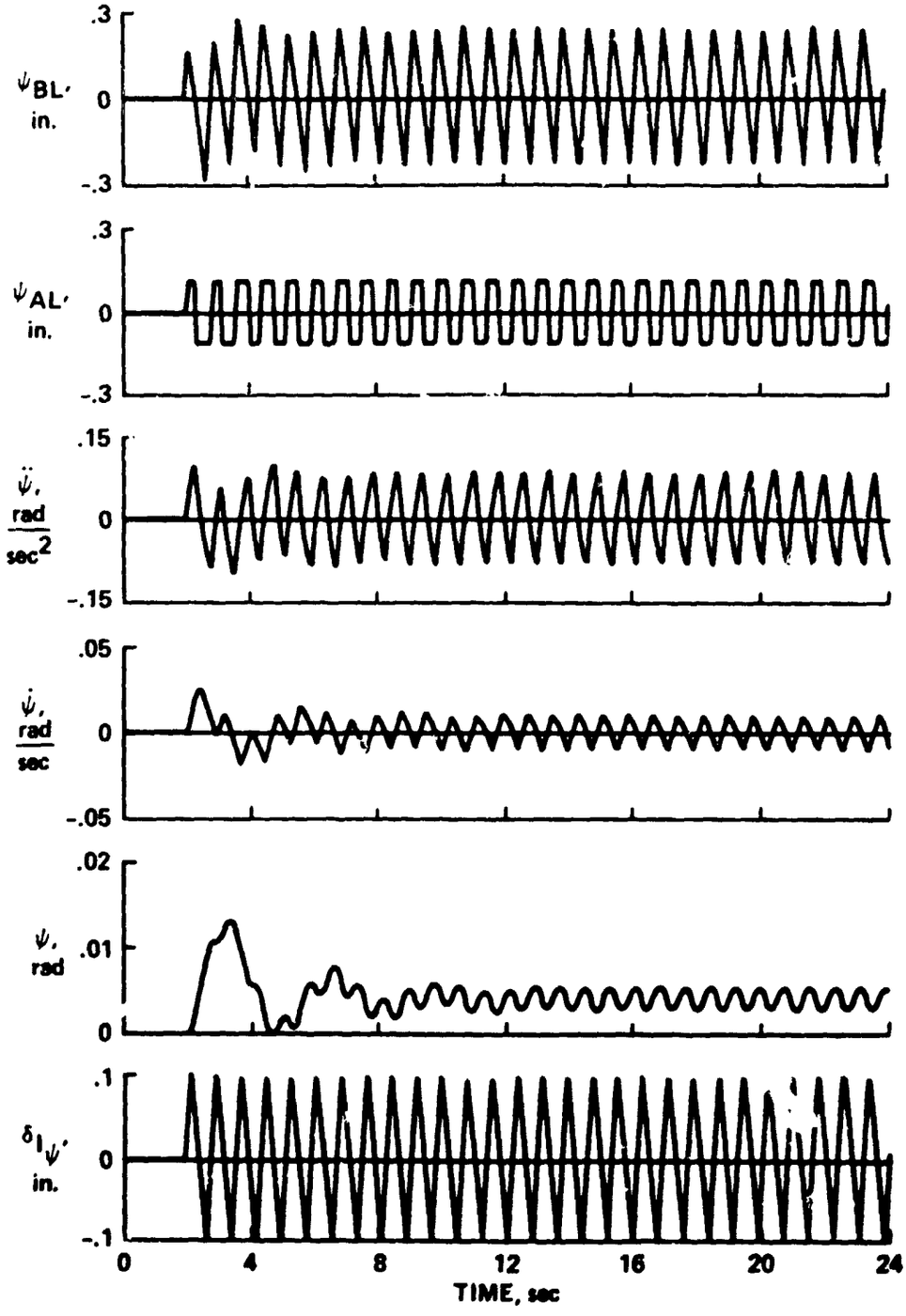

Figure 17.- Nominal configuration, parallel/series servo, $\delta_{I_\psi} = 0.1 \sin(8.0t)$.

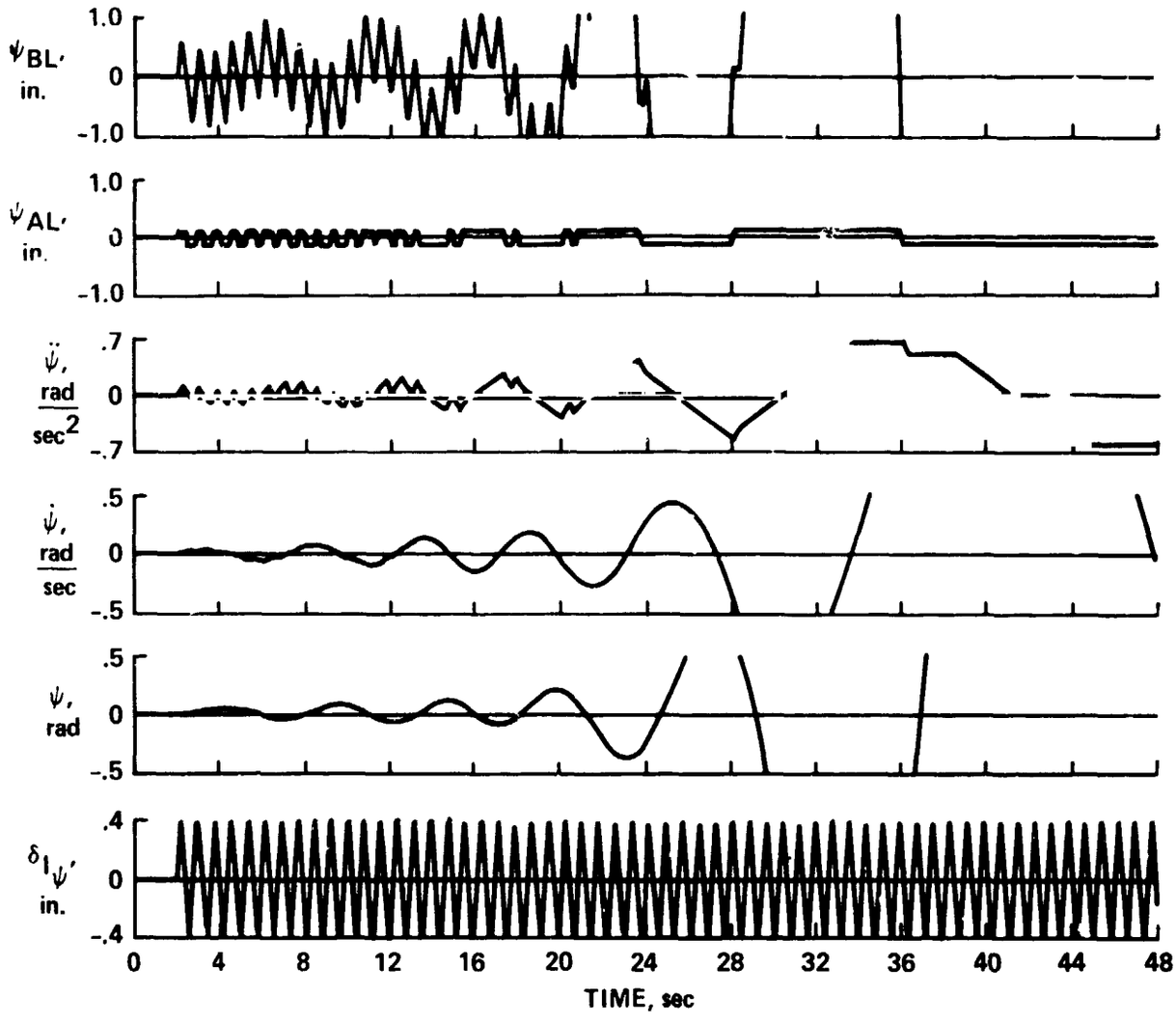

Figure 18.- Nominal configuration, parallel/series servo, $\delta_{I_\psi} = 0.4 \sin (8.0t)$.

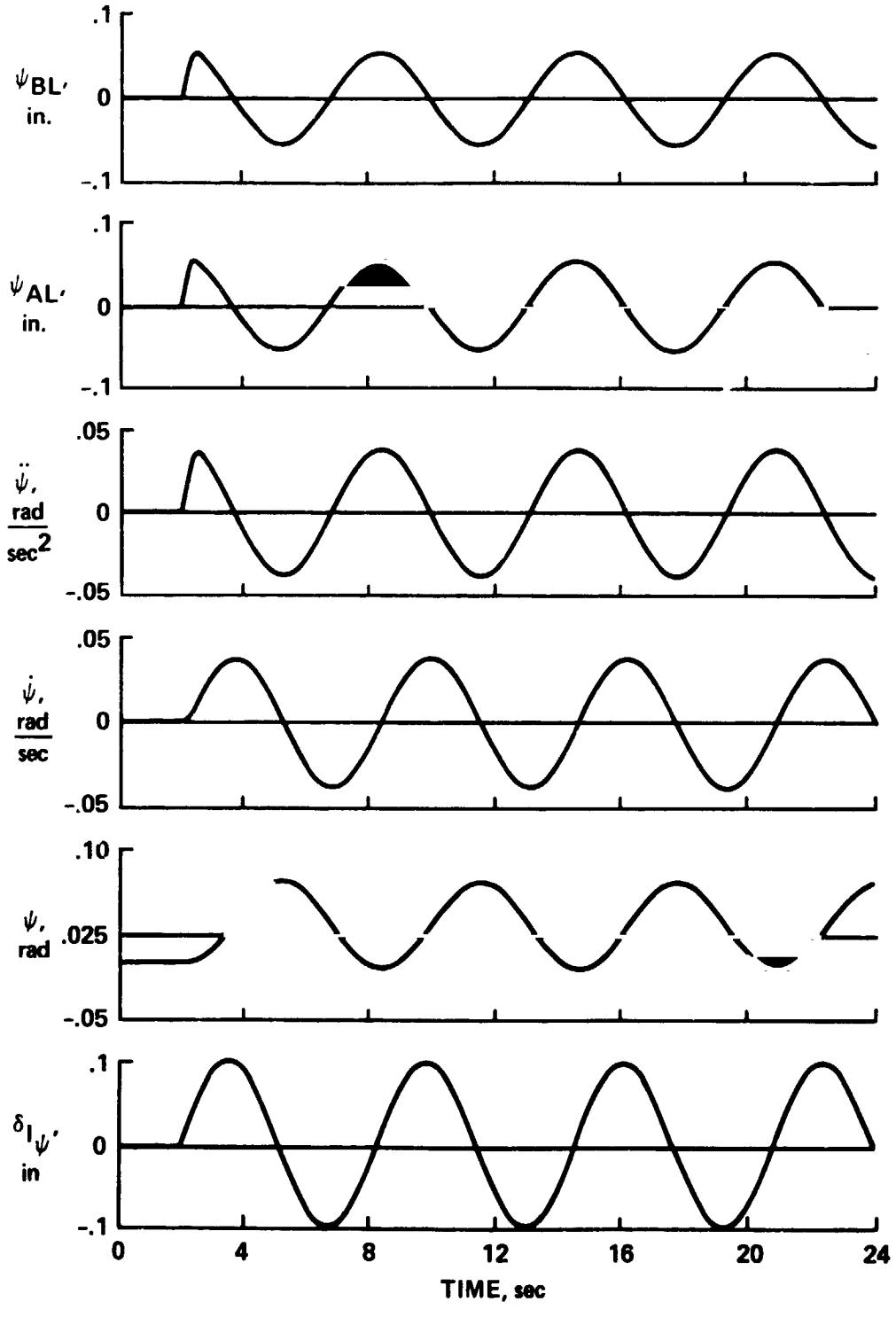

Figure 19.- Nominal configuration, series servo, δ_{I_ψ} = 0.1 sin (1.0t).

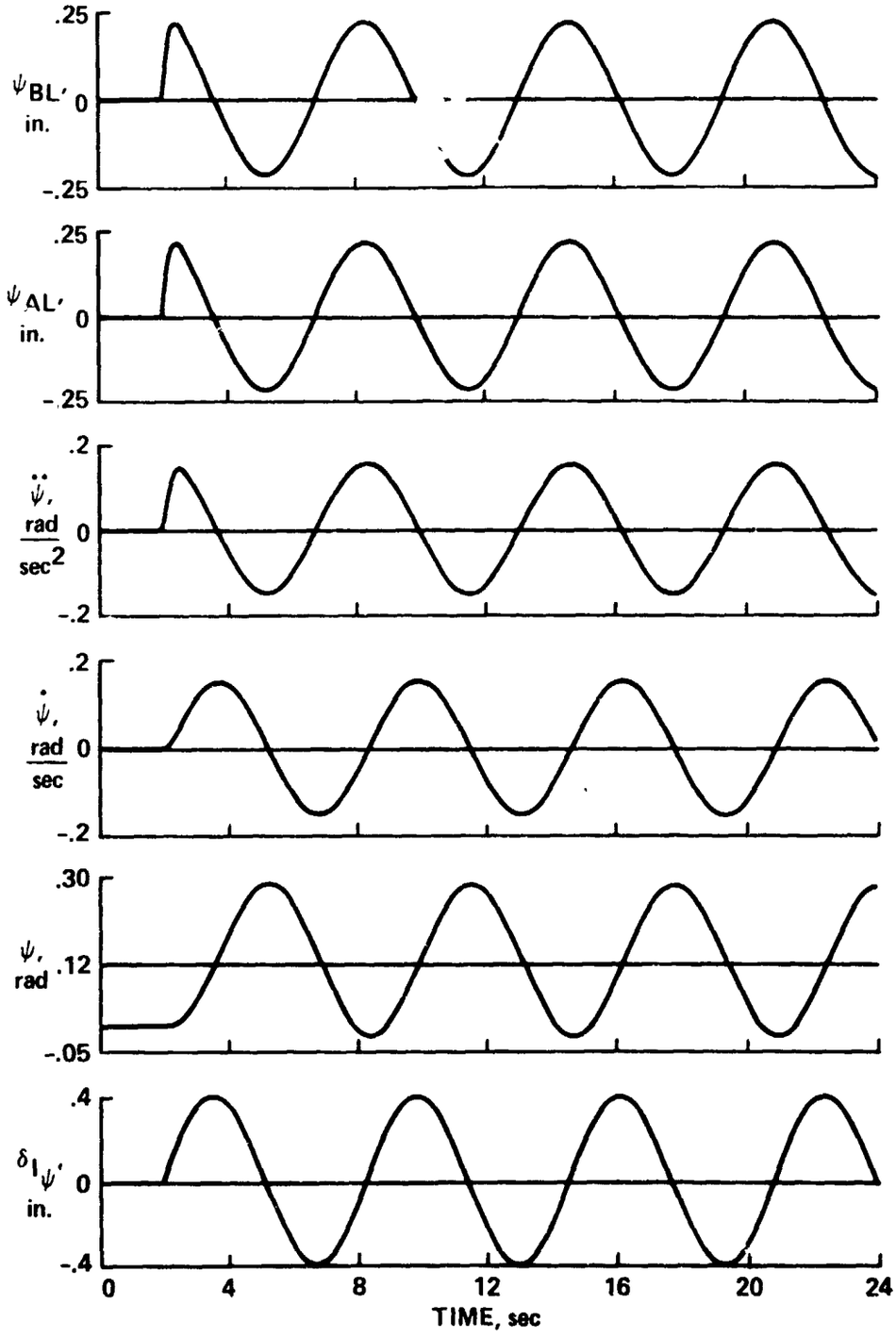

Figure 20.- Nominal configuration, series servo, $\delta_{I_\psi} = 0.4 \sin (1.0t)$.

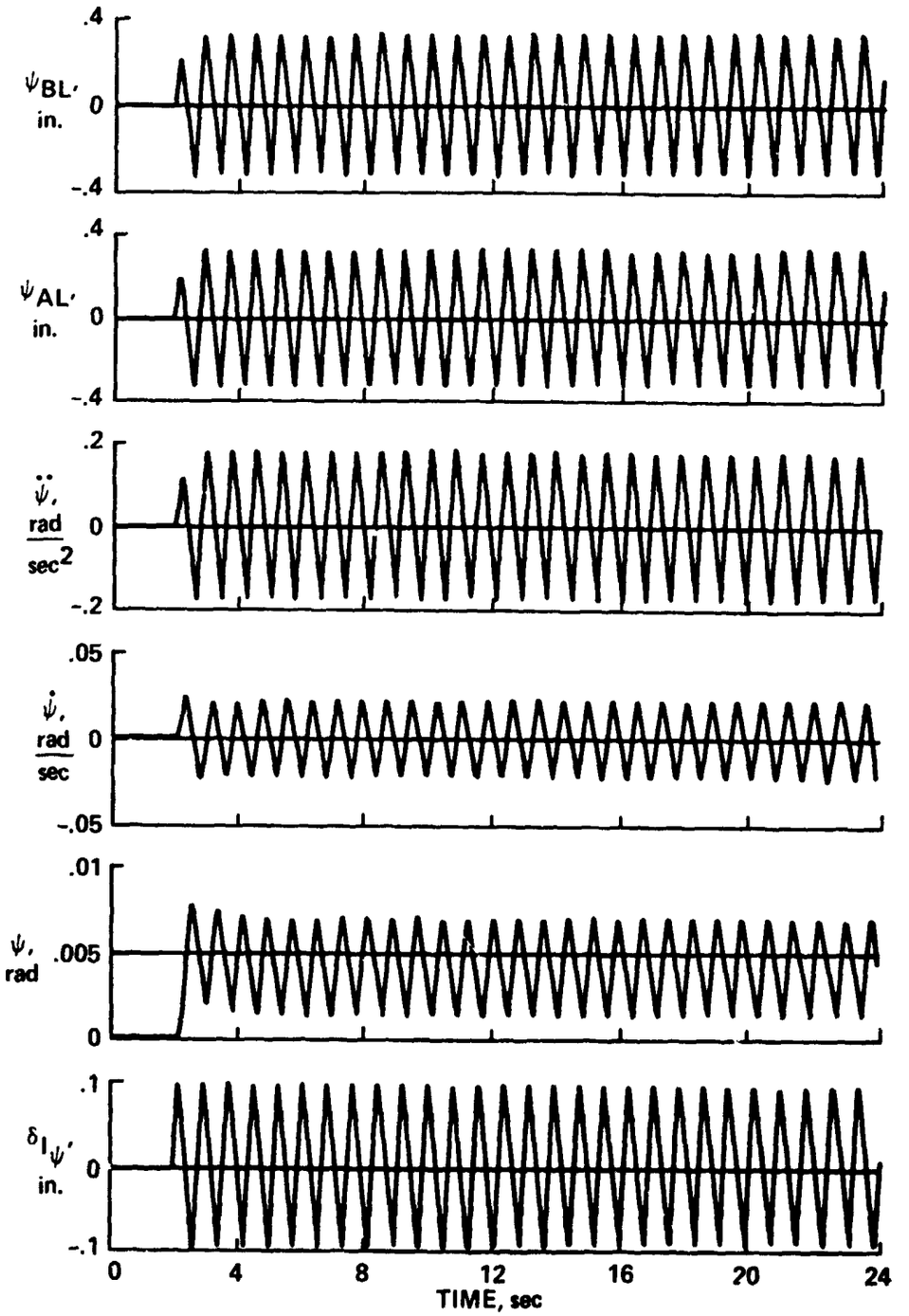

Figure 21.- Nominal configuration, series servo, δ_{I_ψ} = 0.1 sin (8.0t).

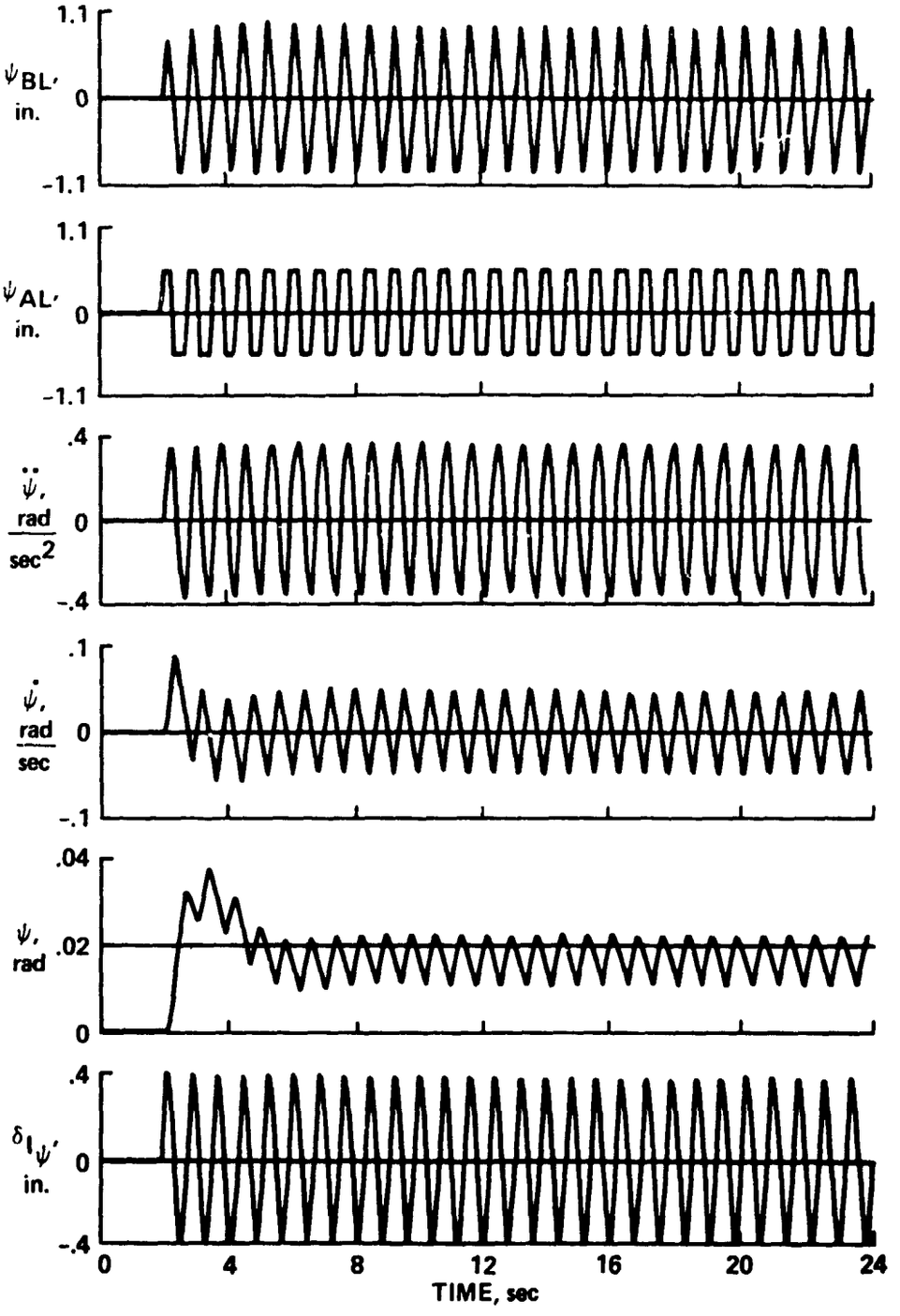

Figure 22.- Nominal configuration, series servo, δ_{I_ψ} = 0.4 sin (8.0t).

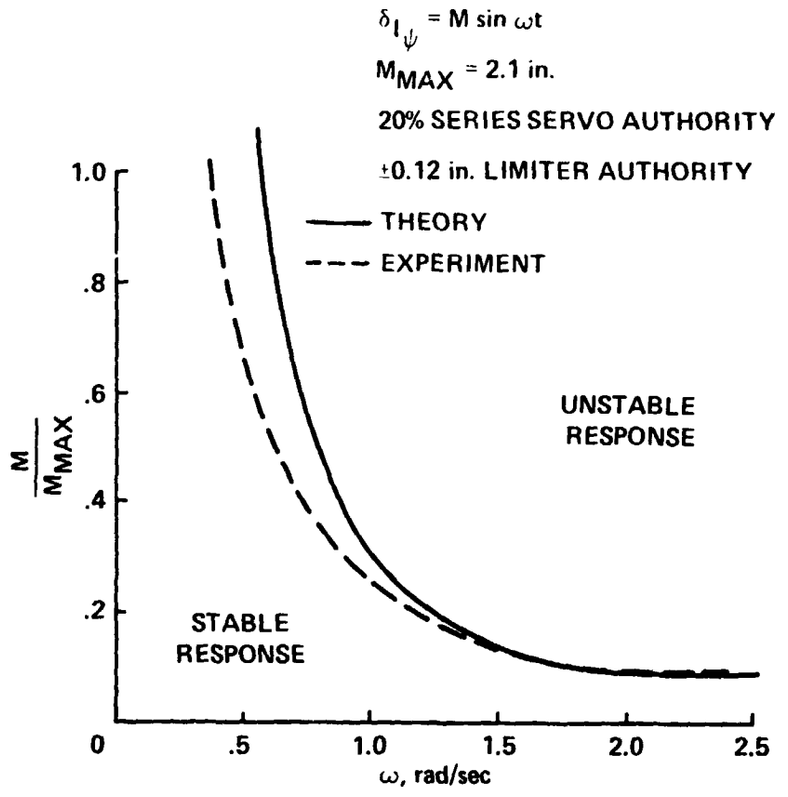

Figure 23.- Amplitude-frequency stability boundary for sinusoidal input.

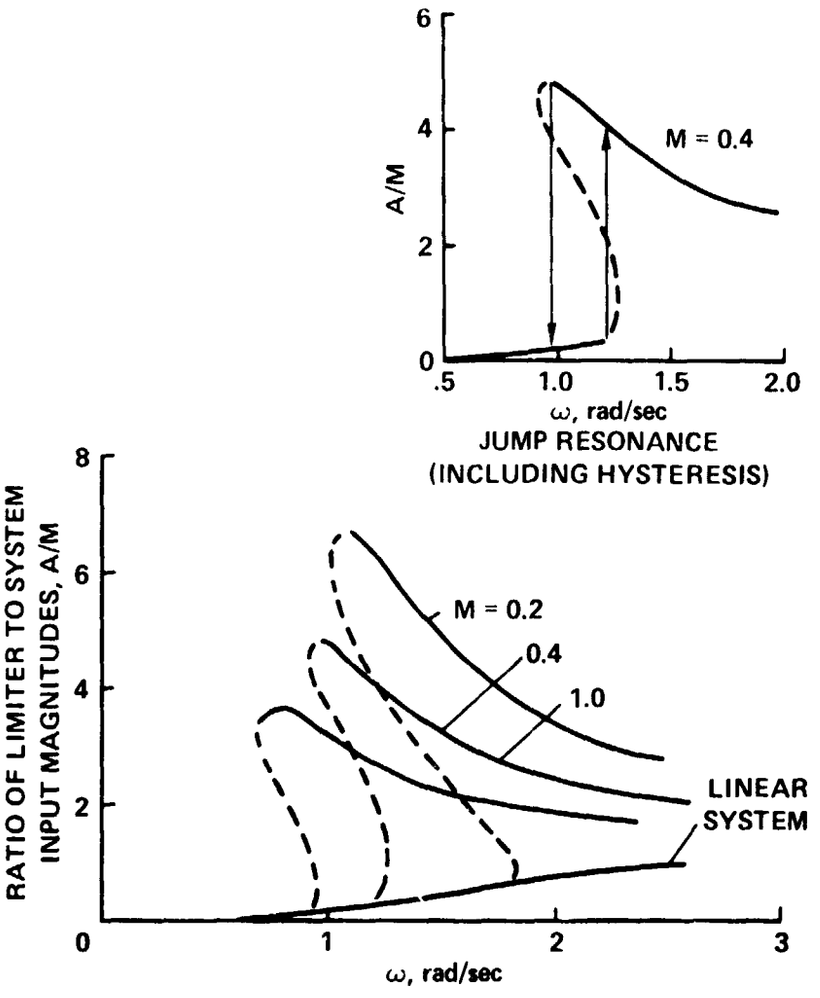

Figure 24.- Frequency response of linear and nonlinear systems; inset shows jump discontinuity upon saturation; system input = δ_{I_ψ} = M sin ωt; 20% series servo authority; ±0.12 in. limiter authority.

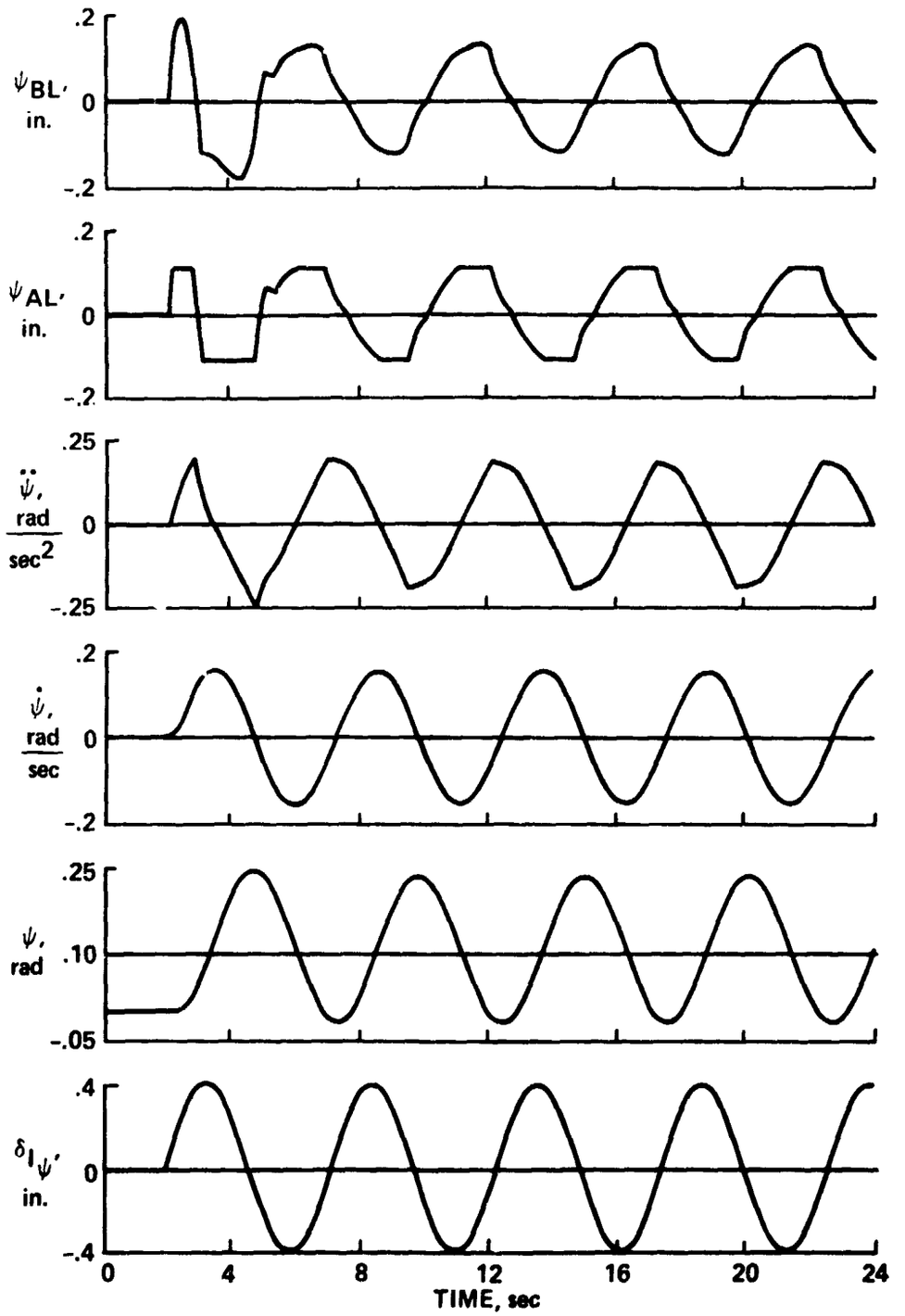

Figure 25.- Nominal configuration, parallel/series servo, $\delta_{I_\psi} = 0.4 \sin (1.22t)$.

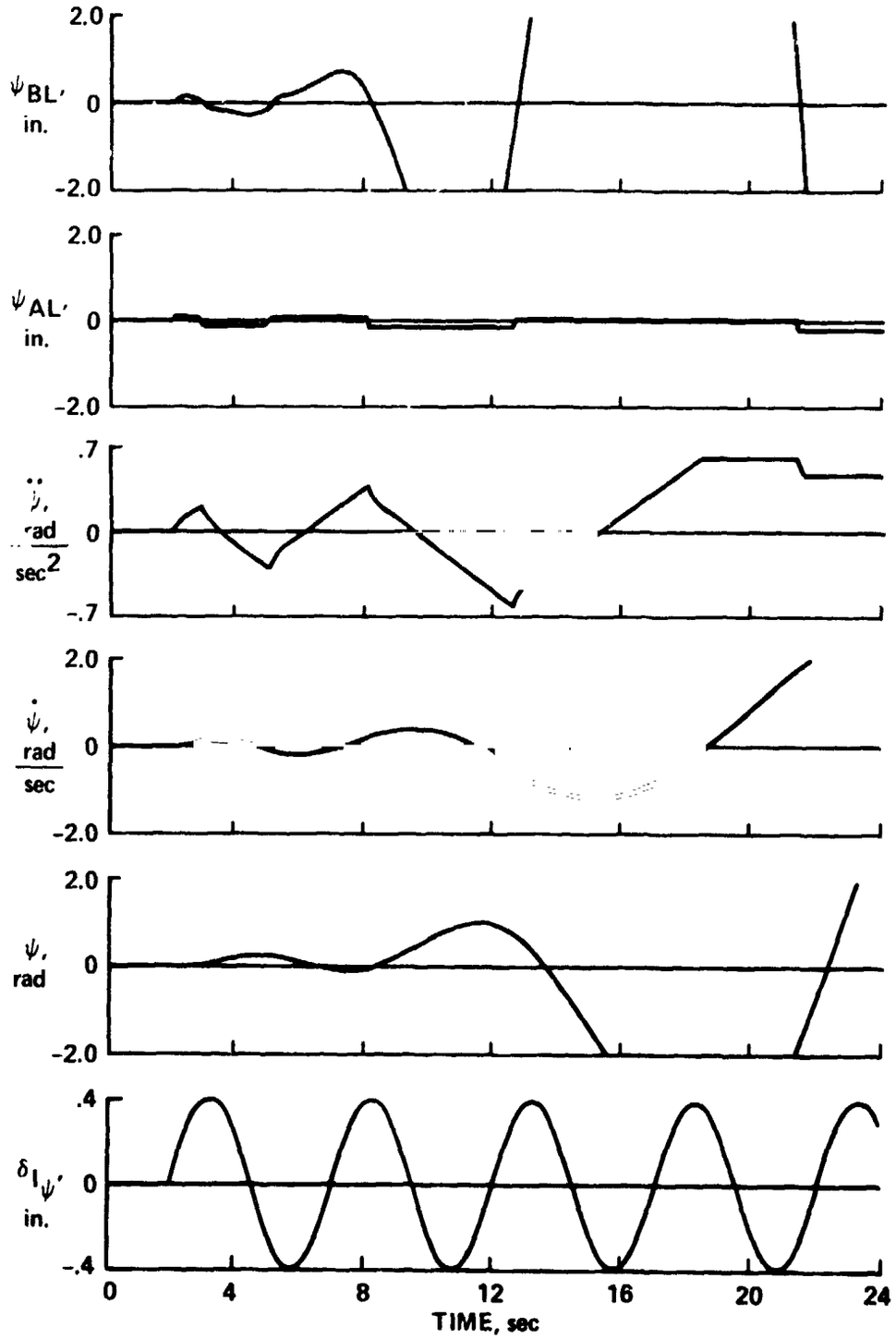

Figure 26.- Nominal configuration, parallel/series servo, $\delta_{I_\psi} = 0.4 \sin (1.25t)$.

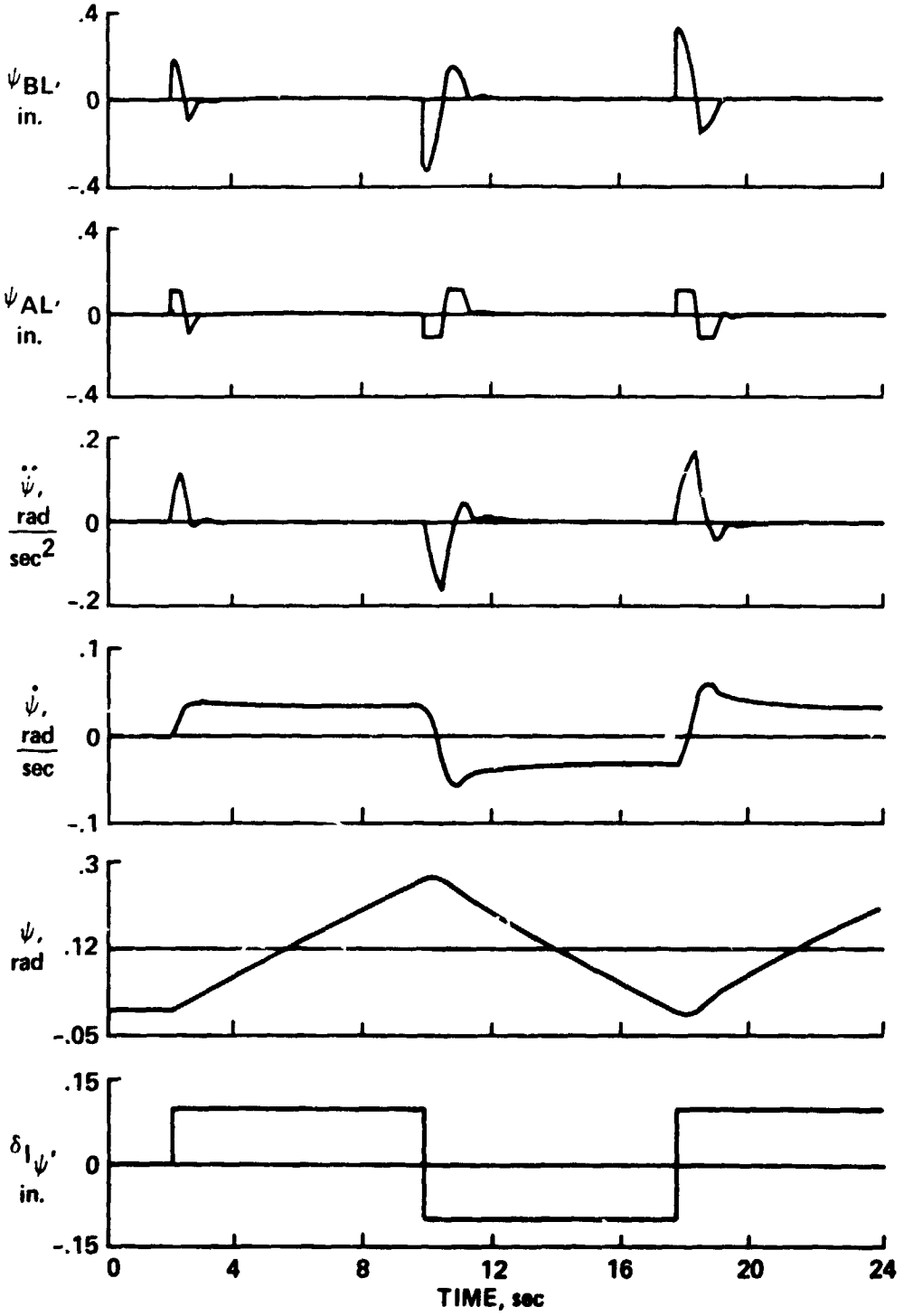

Figure 27.- Nominal configuration parallel/series servo, δ_{I_ψ} = square wave, M = 0.1, ω = 0.4 rad/sec.

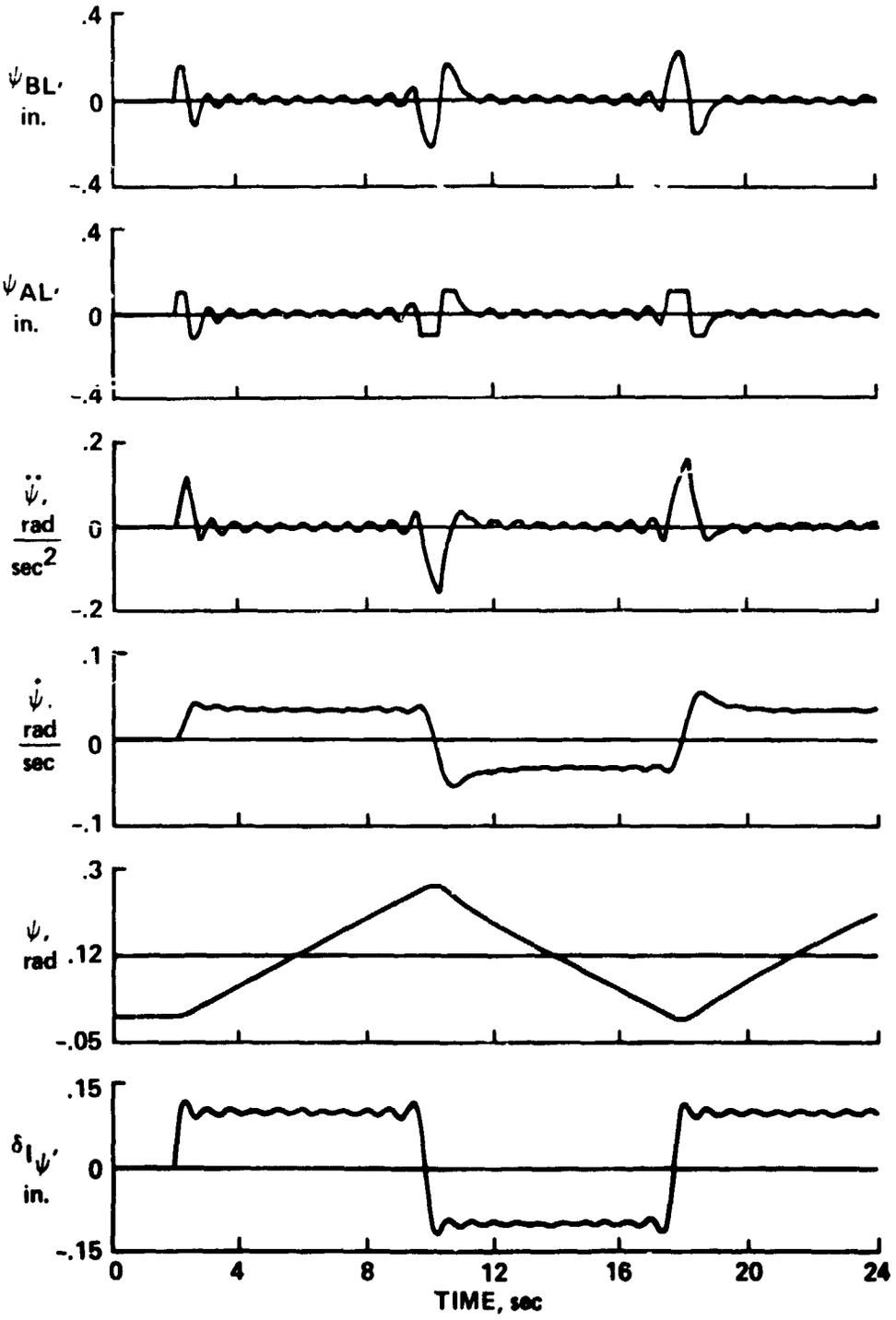

Figure 28.- Nominal configuration, parallel/series servo, $\delta_{I_\psi} = \frac{0.4}{\pi} \sum_{n=1}^{21} \frac{1}{n} \sin(nt)$.

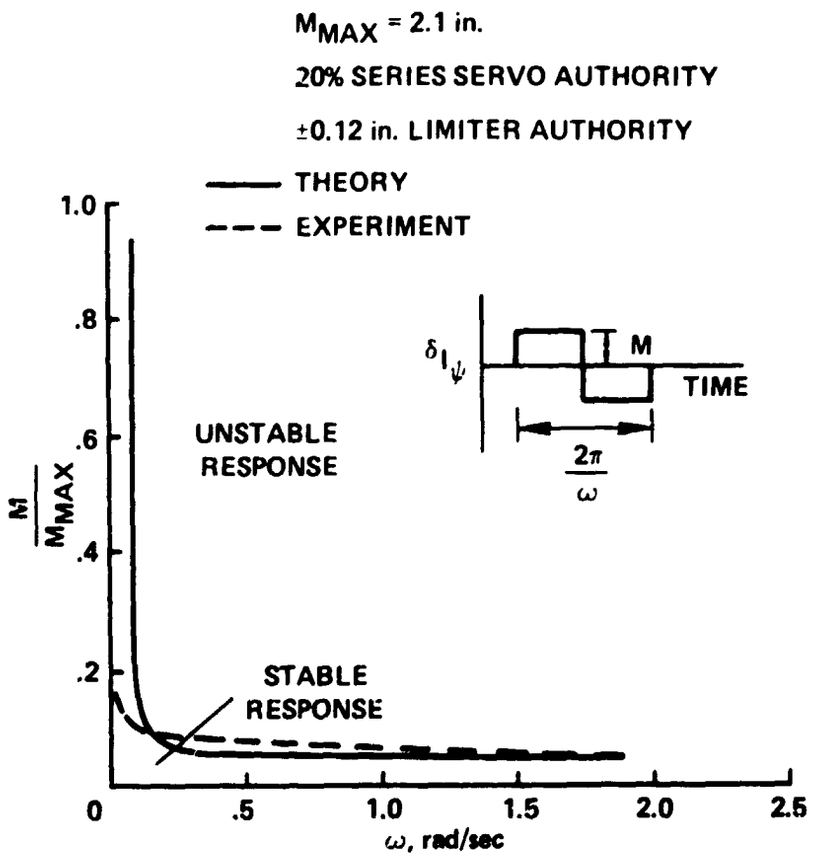

Figure 29.- Amplitude-frequency stability boundary for square wave input.

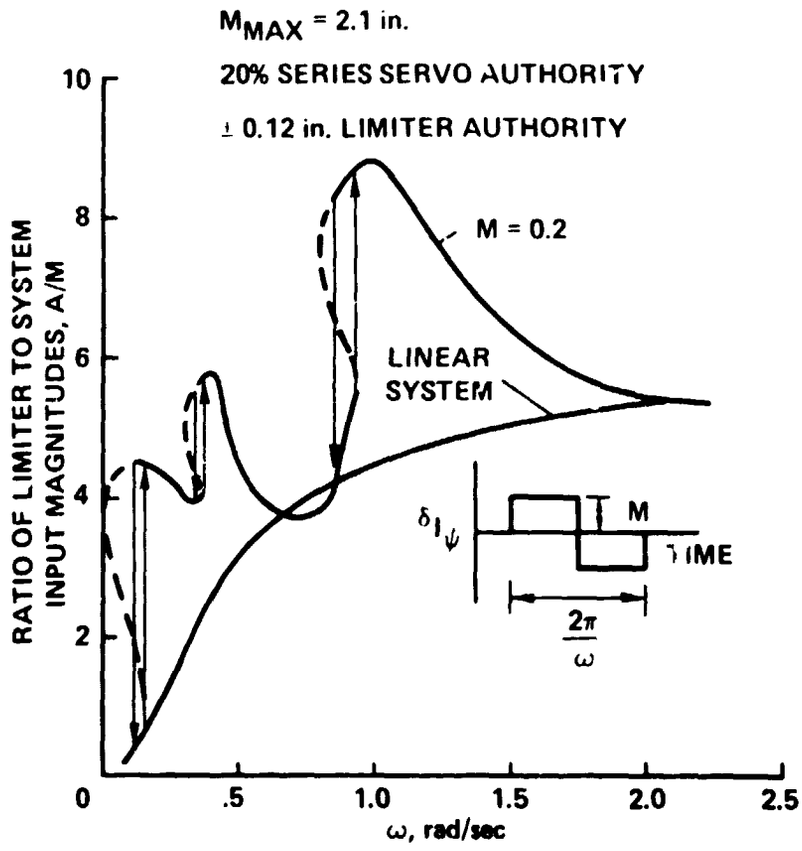

Figure 30.- Frequency response of linear and nonlinear systems, including jump resonance discontinuity upon saturation.

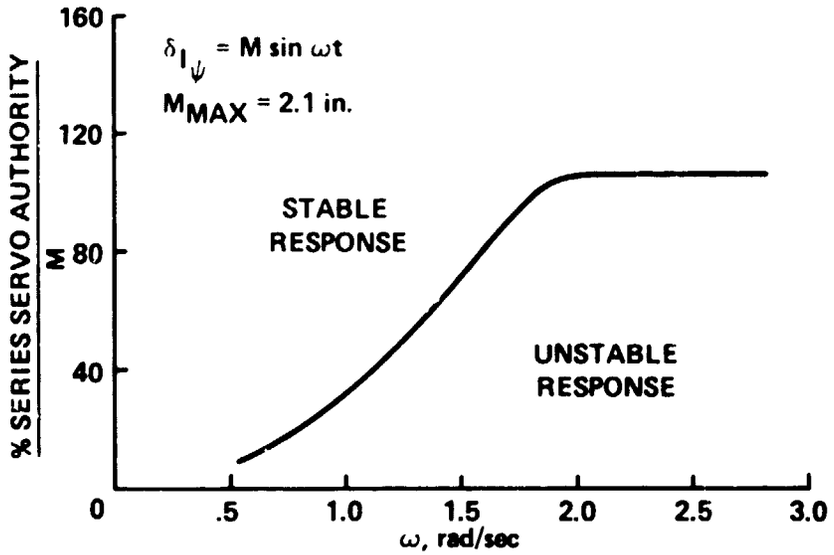

Figure 31.- Stability boundary as a function of normalized series servo authority and input frequency.

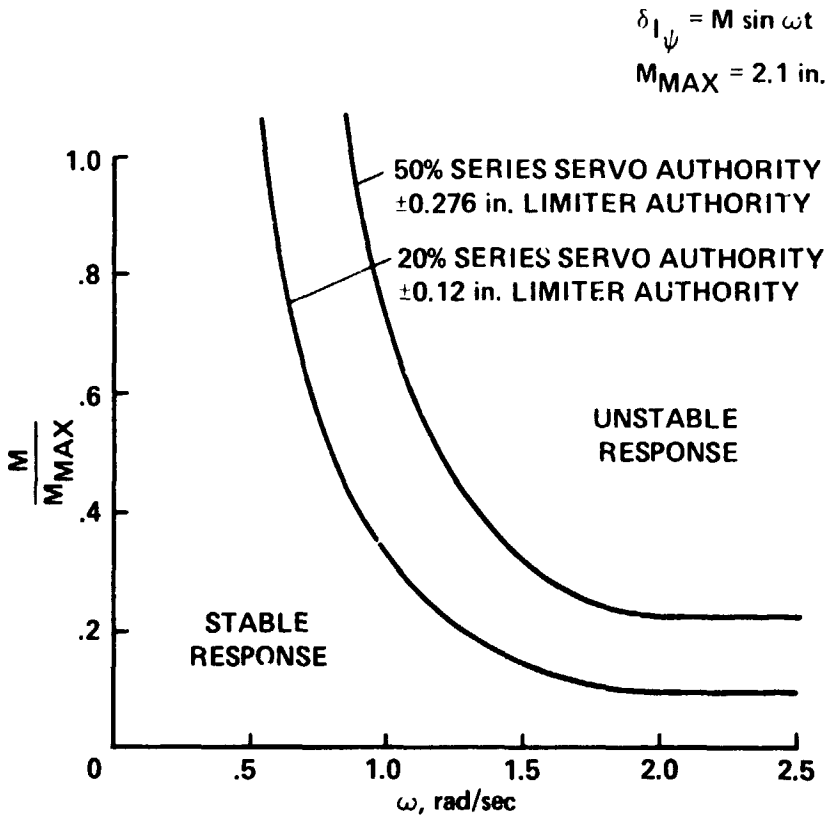

Figure 32.- Amplitude-frequency stability boundary as a function of series servo authority.

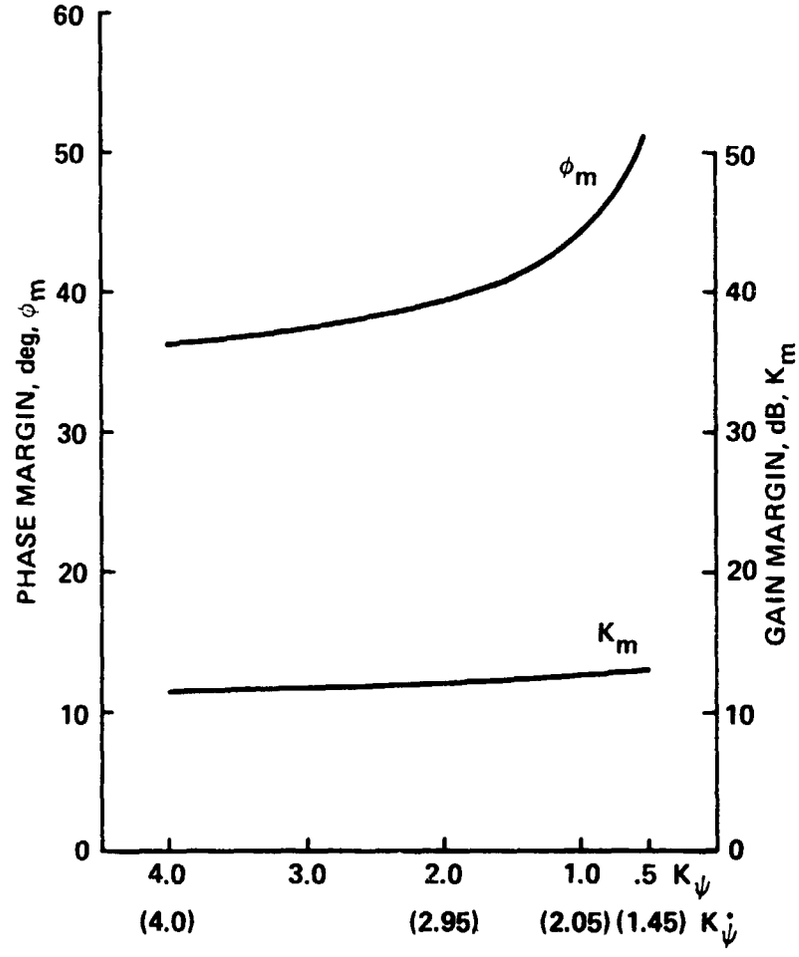

Figure 33.- Variation of linear system phase and gain margins with yaw angle and rate feedback gains, K_ψ and $K_{\dot{\psi}}$.

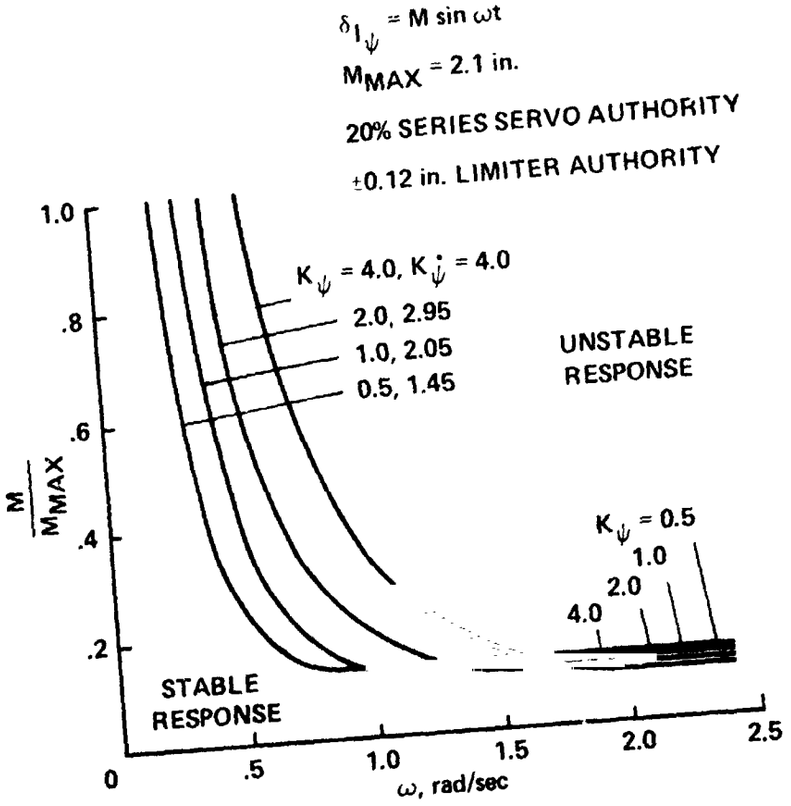

Figure 34.- Amplitude-frequency stability boundary as a function of yaw angle and rate feedback gains, K_ψ and $K_{\dot\psi}$.

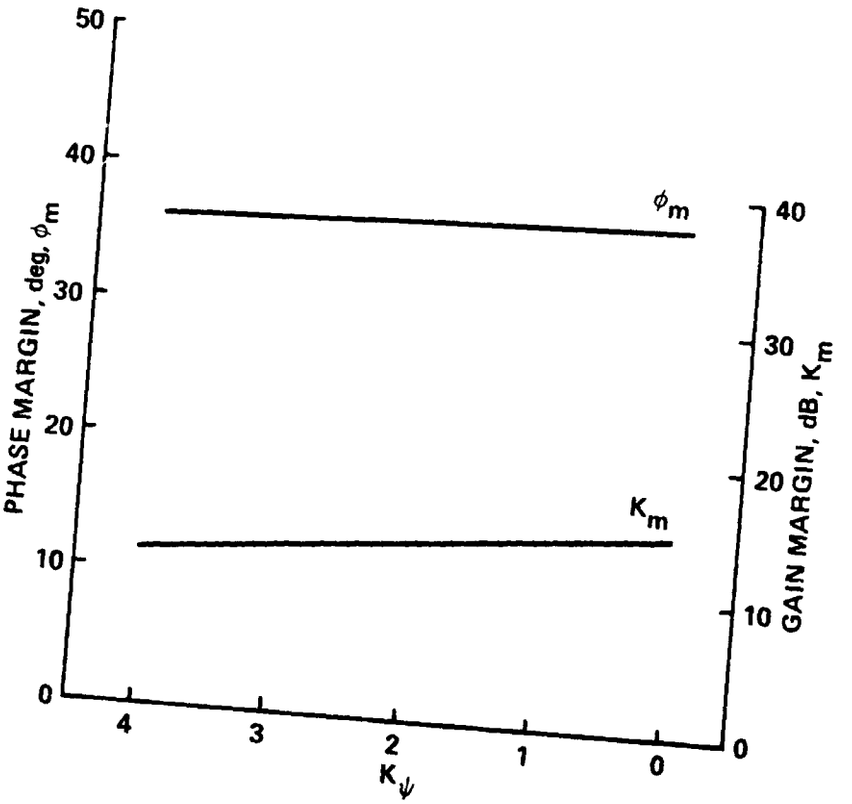

Figure 35.- Variation of linear system phase and gain margins with yaw angle feedback gain, K_ψ.

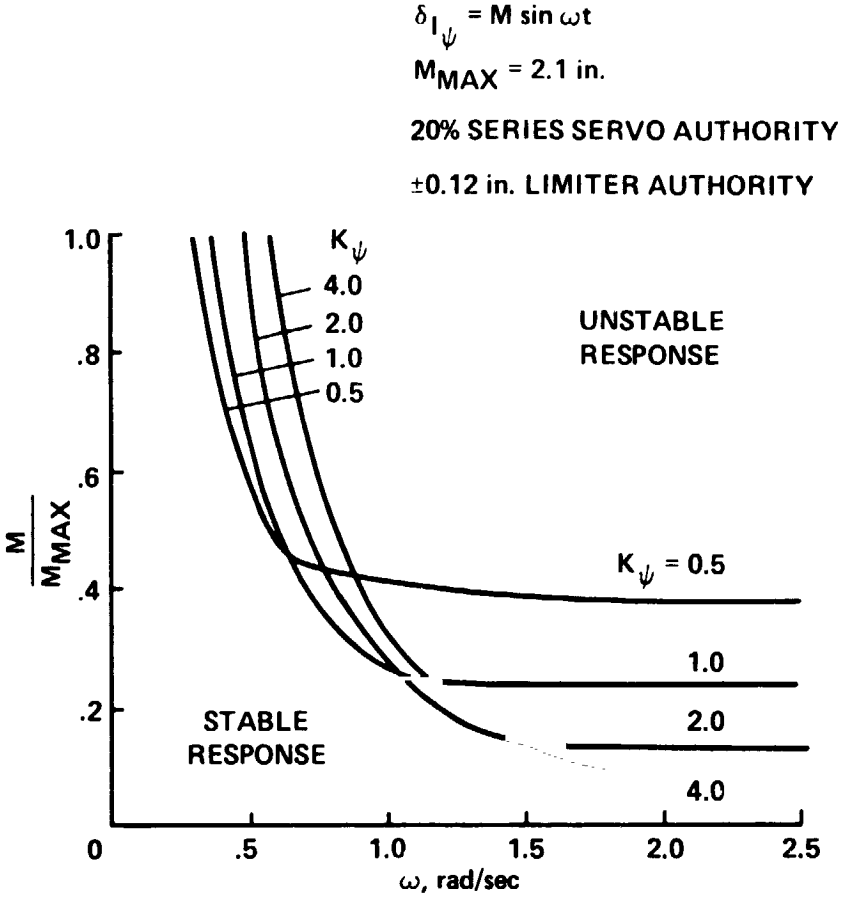

Note: With $K_\psi = 0 \Rightarrow$ stability boundary eliminated.

Figure 36.- Amplitude-frequency stability boundary as a function of yaw angle feedback gain, K_ψ.

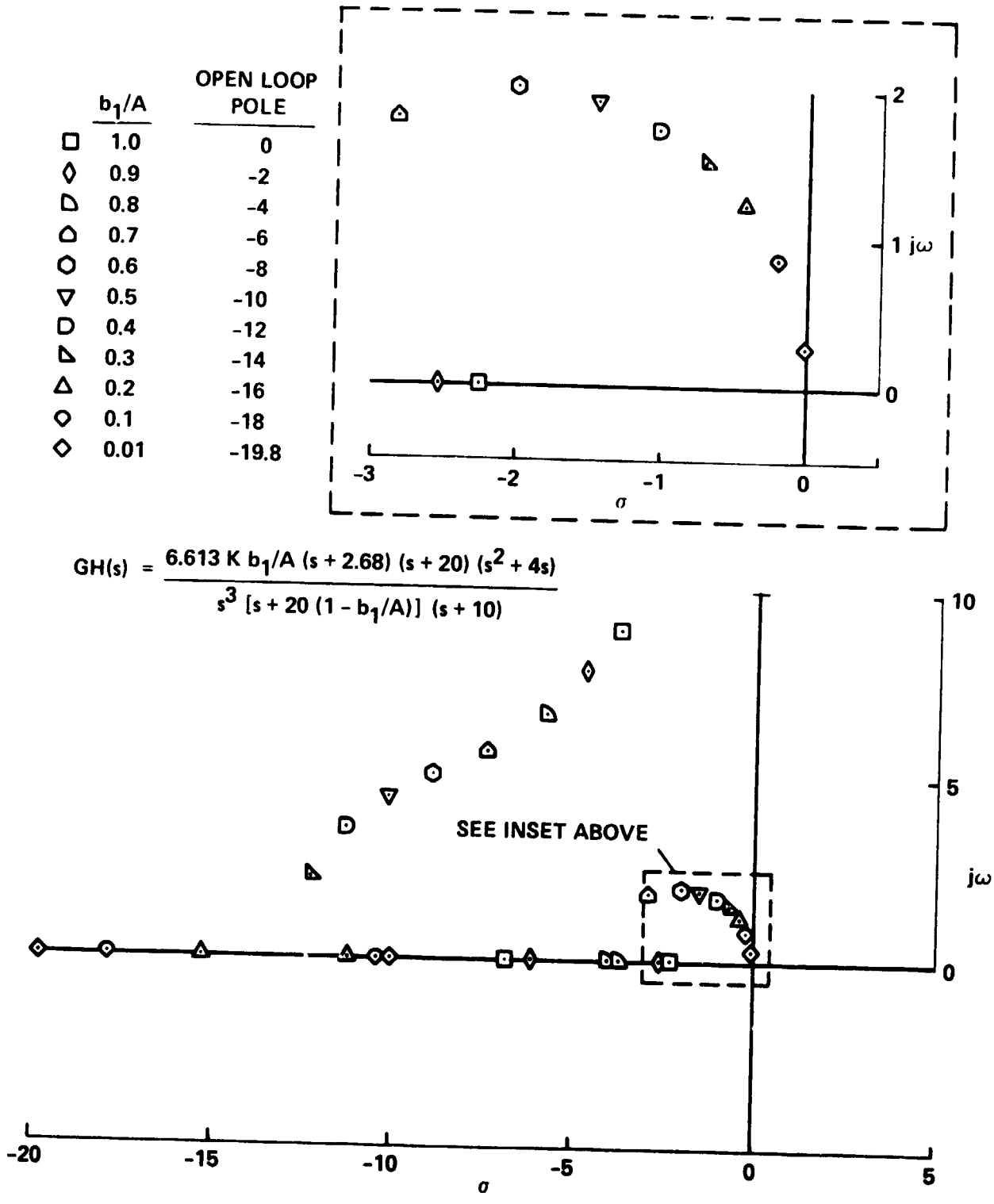

Figure 37.- Variation of closed-loop roots with magnitude of nonlinearity (b_1/A). K_ψ = C, parallel/series servo mode.

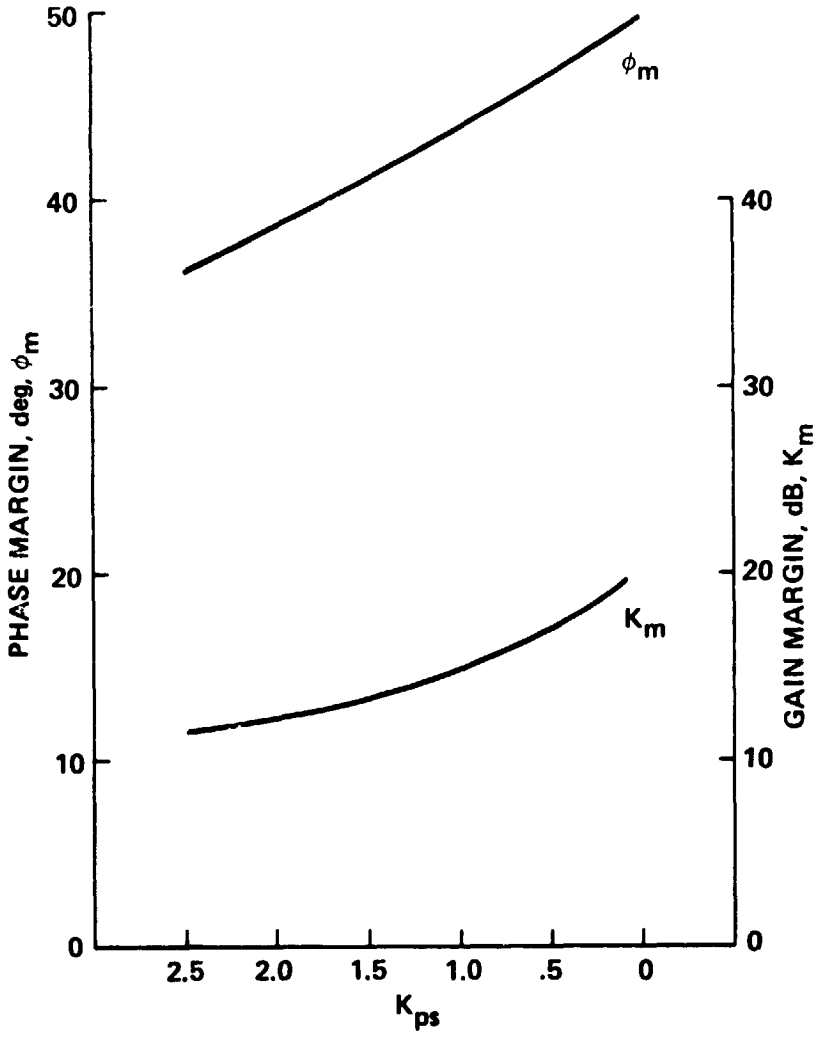

Figure 38.- Variation of linear system phase and gain margins with parallel servo gain, K_{ps}.

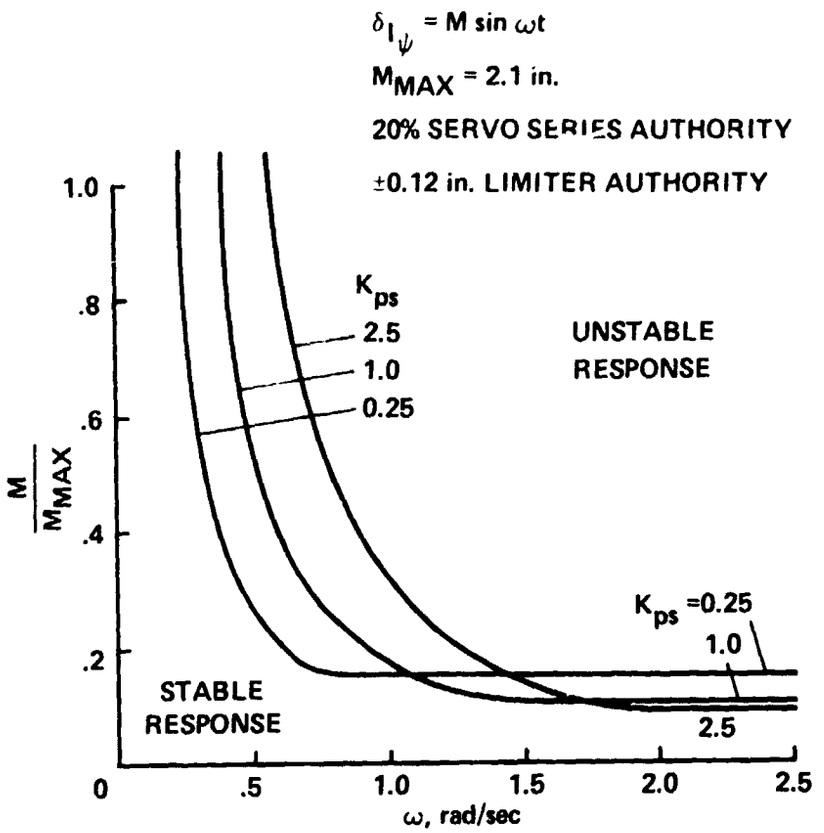

Figure 39.- Amplitude-frequency stability boundary as a function of parallel servo gain, K_{ps}.

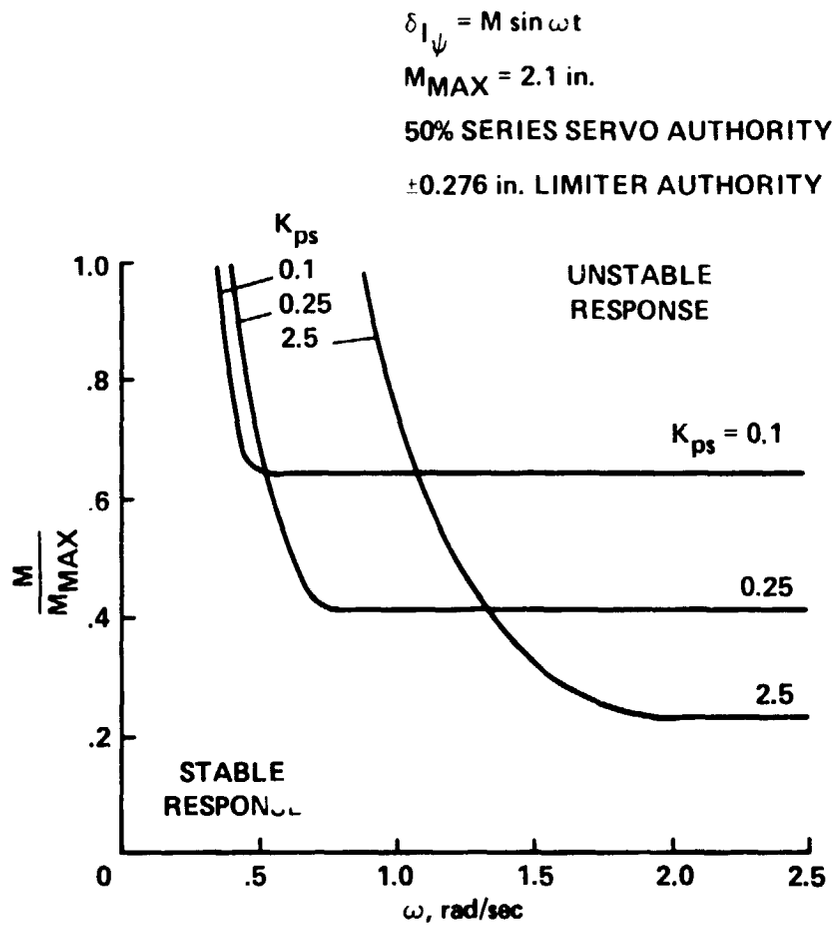

Figure 40.- Amplitude-frequency stability boundary as a function of parallel servo gain, K_{ps}.